AEA Technology
Materials & Chemistry Division

A One-Dimensional Thermal Model of a TOPAZ-II TFE

J.L. Ing and P. Agnew

Work undertaken for the European Office of Aerospace Research and Development of the U.S. Air Force under contract number F61708-95-C0002.

13th September 1995

P. Agnew
TOPAZ International Program
901 University Blvd.
Albuquerque, NM 87106
USA.

REPORT DOCUMENTATION PAGE

Form Approved OMB No. 074-0188

1. AGENCY USE ONLY (Leave blank)	2. REPORT DATE 13 September 1995	3. REPORT TYPE AND DATES COVERED Final Report

4. TITLE AND SUBTITLE A One-Dimensional Thermal Model of a TOPAZ-II TFE

5. FUNDING NUMBERS F61708-95-C0002

6. AUTHOR(S)
Agnew, P.; Ing, J.

7. PERFORMING ORGANIZATION NAME(S) AND ADDRESS(ES)

AEA Technology
Materials & Chemistry Division
Didcot
United Kingdom

8. PERFORMING ORGANIZATION REPORT NUMBER

9. SPONSORING / MONITORING AGENCY NAME(S) AND ADDRESS(ES)

EOARD
PSC 802 Box 14
FPO 09499-0200

10. SPONSORING / MONITORING AGENCY REPORT NUMBER
SPC 98-4005-4

11. SUPPLEMENTARY NOTES

12a. DISTRIBUTION / AVAILABILITY STATEMENT Approved for public release; distribution is unlimited.

12b. DISTRIBUTION CODE

13. *ABSTRACT* (Maximum 200 Words)

14. SUBJECT TERMS Foreign Reports, EOARD

NUMBER OF PAGES 44

16. PRICE CODE

17. SECURITY CLASSIFICATION OF REPORT	18. SECURITY CLASSIFICATION OF THIS PAGE	19. SECURITY CLASSIFICATION OF ABSTRACT	20. LIMITATION OF ABSTRACT
UNCLASSIFIED	UNCLASSIFIED	UNCLASSIFIED	UL

Section 1 - TFE 1-D Thermal Model

1.1. Introduction

The TOPAZ-II space nuclear reactor, Ya-21u, was tested as part of the Topaz International Program in Albuquerque, NM during the period August 1993 to March 1995. It was also tested in Russia prior to its arrival in the U.S. Thermal testing was carried out using tungsten electrical heaters (TISA heaters) to simulate the nuclear fuel. No nuclear testing has been carried out on this system. Details of the TOPAZ-II reactor are given by the U.S. TOPAZ-II Flight Safety Team (1992), Wold *et. al.* (1994) and Paramonov and El-Genk (1994). During the testing of Ya-21u, the reactor was subjected to a variety of extreme conditions, including a shake and vibration test, air leaks into the TFEs and thermal shocks. Details of U.S. testing of Ya-21u are given by Schmidt *et. al.* (1995). Over the duration of these tests the electrical output parameters of the reactor changed significantly, presumably as a result of changes to internal TFE parameters such as effective emissivity of the inter-electrode gap, emitter and collector work functions and gap dimensions. The individual TFE characteristics depend sensitively on these parameters and the final electrical output is the result of a delicate balance between a number of competing effects. In order to better understand the factors resulting in the output degradation it proved necessary to develop computer models of the various internal TFE processes. An additional need arose to determine the effect of changes in NaK coolant temperature, such as occurred when the reactor was run without the radiator thermal shield. The computer codes described in this report were developed to meet these needs. Their primary function is to model heat transfer and thermionic emission within a single TFE. The theoretical treatment is exclusively one dimensional. This limitation is not thought to be particularly important for our primary applications. There is no doubt that a one dimensional treatment is capable of indicating qualitative trends in the variation of parameters, and the quantitative limitations of a one dimensional treatment (due to TFE 'end effects') are not too severe, in view of the actual TFE geometry. In our models heat transfer within the TFE is calculated out to the NaK coolant channel and the temperature here is used as a boundary condition. A more comprehensive model of the entire reactor system, including coolant flow and reactor neutronics, is described by Paramonov and El-Genk (1994). However this degree of sophistication is not necessary for the applications described above. By eliminating details of the rest of the reactor systems it has been possible to work with more detailed and realistic codes for generating the current-voltage characteristics of TFEs under a given set of operating conditions. This in turn should lead to more reliable estimates of internal TFE parameters.

1.2. Theory

The heat transfer models combine the thermionic emission process with the heat transfer properties of the TFE. They calculate the output current density (J_{out}) given the input thermal power (q_{FUEL}), output volts (V_{out}), cesium pressure (P_{Cs}) and NaK flow rate ($\dot{m}$). Unless the reactor is running at very low current densities, the heat transfer across the electrode gap as a result of the transfer of electrons from the emitter to the collector is a significant proportion of

the total heat transfer. The electron current is a very sensitive function of temperature in the TFE, especially the emitter temperature. Hence an iterative procedure is required to calculate the temperatures of the components of the TFE and the output current for a given set of operating conditions. This procedure alternately balances the heat fluxes into and out of each electrode.

Three codes are described in the following work. These are IV1D, EQ1D and NAK1D. IV1D is a program for calculating I-V characteristics only, given the emitter and collector temperatures (T_E, T_C), P_{Cs}, and V_{out}. It has the option to allow for voltage drops in the electrodes, due to resistive losses. For this it also needs a value for the NaK temperature (T_{NaK}), which is used in calculating the resistivity of the electrodes along their entire length. It does not consider heat transfer nor calculate equilibrium temperatures. EQ1D is used in calculating equilibrium values of T_E, T_C and J_{out} in operating conditions similar to those used on Ya-21u. It is used to produce a calibration between the heat flux to the NaK (Q_{NaK}) and T_{NaK}, from experimental data of the relationship between q_{FUEL} (for 1 TFE) and T_{NaK} (see section 1.2.2). NAK1D is the most general program, calculating equilibrium values of T_E, T_C, T_{NaK} and J_{out} in a TOPAZ-II TFE under any physically reasonable operating conditions. It then allows the user to change T_{NaK} and calculate the new equilibrium conditions. This is useful for considering the changes which occurred when Ya-21u was run without the thermal shield, resulting in NaK temperatures up to ~ 60 K lower than when the thermal shield was in place. Both heat transfer models use the same IV characteristic code as IV1D. The main components of the model are described below in section 1.2.2.

1.2.1 Units

Unless otherwise stated, the following units have been used in this work, in both the codes and the theory described below:

Quantity	**Symbol**	**Units**
Temperature	T	K
Current density	J	A cm^{-2}
Current	I	A
Voltage	V	V
Work function	ϕ	eV
Power	q	W
Heat flux	Q	W cm^{-2}
Area	A	cm^2
Length	l	cm
Radius, diameter	r, d	cm
Gap spacing	d	cm
Pressure	P	Torr
Thermal conductivity	k, λ	W cm^{-1} K^{-1}
Electrical resistivity	ρ	Ω cm
Specific heat capacity	c_P	J $kg^{-1}K^{-1}$
Mass flow rate	$\dot{m}$	kg s^{-1}

1.2.2 Heat transfer

The heat transfer models NAK1D and EQ1D both find equilibrium conditions by using a Newton-Raphson routine to adjust the temperature of each electrode until the heat flux into the electrode equals that out of the electrode. This is done alternately for the emitter and collector until the temperatures and output current converge. The heat flux (i.e. power per unit area) from the TISA to the inner surface of the emitter (Q_{FUEL}) is calculated from q_{FUEL}. The active length of the TFE, over which heat transfer from the TISA has been assumed to take place, l, is 30 cm. The loss from q_{FUEL} as a result of resistive losses in the leads is taken as 12% (Steppenov 1991). The radii of the TFE components are shown in figure 1.1 (Paramonov and El-Genk 1994).

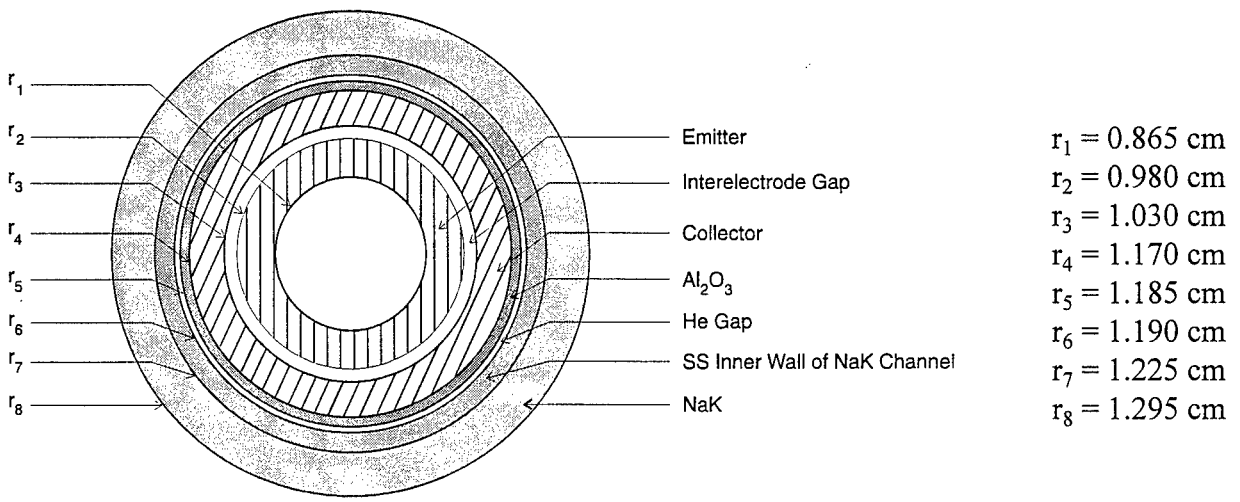

Figure 1.1: Radii of TOPAZ-II TFE components.

Hence Q_{FUEL} is given by

$$Q_{FUEL} = \frac{0.88 q_{FUEL}}{2\pi r_2 l} \quad . \tag{1.1}$$

Three mechanisms of heat transfer from the emitter to the collector are significant. From largest to smallest these are radiative, electron transfer and conductive heat transfer through the Cs vapour. Since the heat transfer via electron transfer is significant under typical TFE operating conditions, this effectively couples the heat transfer and I-V characteristic parts of the model. The radiative heat transfer Q_{rad} is given by

$$Q_{rad} = \sigma \varepsilon_{eff} \left(T_E^4 - T_C^4 \right) \ , \tag{1.2}$$

where σ is the Stefan-Boltzmann constant and ε_{eff} is the effective emissivity of the inter-electrode gap. This depends on the emissivities of both the collector and the emitter. The values used for ε_{eff} are discussed in section 1.2.2.1.

The heat flux from the emitter due to electron cooling, Q_{eE}, depends on the mode in which the TFE is operating (McVey and Rasor, Dahlberg *et. al.* 1994, Rasor Associates 1991). Q_{eE} is calculated in the IV characteristic part of the program and will not be discussed further here.

The corresponding heat flux due to electron heating of the collector, Q_{eC}, is given by

$$Q_{eC} = Q_{eE} - J_{out}V_{out} \quad . \tag{1.3}$$

The heat flux due to conduction through the Cs vapour, Q_{Cs}, is given by Hatsopoulos and Gyftopoulos (1973) as

$$Q_{Cs} = \frac{\lambda_{mw}(T_{mw})(T_E - T_C)}{d + 1.15\times10^{-5}\left[(T_E + T_C)/P_{Cs}\right]} \quad , \tag{1.4}$$

where d is the emitter-collector spacing in cm, and $\lambda_{mw}(T_{mw})$ is the thermal conductivity of Cs. This is a function of the weighted mean temperature T_{mw}, given by Hatsopoulos and Gyftopoulos (1973) as

$$T_{mw} = \frac{4}{9}\left(\frac{T_E^{\frac{3}{2}} - T_C^{\frac{3}{2}}}{T_E - T_C}\right)^2 \quad . \tag{1.5}$$

The variation of λ_{mw} with T_{mw} is shown in figure C10, together with the analytical expression representing this data.

Heat transfer from the collector to the NaK is dominated by conduction, since the temperatures are much lower than at the emitter. Only conduction has been considered in these models. Conduction through the plasma-sprayed Al_2O_3 collector coating, the He gap and the stainless steel inner wall of the NaK channel have been considered. Finally, the convective heat transfer to the NaK must be included. Of these contributions, the He gap provides the greatest thermal resistance. Conduction through this layer structure is best described by combining the thermal conductivities of each layer into one parameter. Hence an effective thermal conductivity per unit length of the active zone of the TFE, K_{mean}, is defined such that

$$Q_{NaK} = K_{mean}(T_C, T_{NaK})(T_C - T_{NaK}) \quad . \tag{1.6}$$

K_{mean} is a function of both T_C and T_{NaK}, since the thermal conductivities of the components between the collector and NaK channel are all functions of temperature. Each of the components can be thought of as a thermal resistance. For conduction in the alumina, He and stainless steel, the resistance of that element, R_n, is given by Kreith and Black (1980) as

$$R_n = \frac{\ln(r_{n+1}/r_n)}{2\pi k_n l} \quad , \tag{1.7}$$

where l is the length over which conduction takes place (i.e. the active zone of the TFE) and k_n is the thermal conductivity of that material. With reference to with figure 1.1, the value of n is 4 for the alumina, 5 for the He and 6 for the stainless steel layer. Plots of the thermal conductivity for alumina (Paramonov and El-Genk 1994), He (CRC 1976) and stainless steel (Grigorieva and Melikhova 1991), as a function of temperature, are shown in figures C5, C6 and C7 respectively. The analytical expressions representing these data, which have been used in the codes, are also shown. The thermal resistance of convective heat transfer to the NaK, R_7, is given by Kreith and Black (1980) as

$$R_7 = \frac{1}{2\pi r_7 l h} \quad . \tag{1.8}$$

The method for calculation of h, the convective heat transfer coefficient to the NaK, is given in Appendix A. The total power transferred to the NaK, q_{NaK}, is given by Kreith and Black (1980) as

$$q_{NaK} = \frac{T_C - T_{NaK}}{\sum_{n=4}^{7} R_n} \tag{1.9}$$

If the surface area of all the components is taken to be $2\pi r_7 l$ (i.e. neglecting the difference in surface area of the different layers) and equation 1.9 is substituted in equation 1.6, K_{mean} is given by

$$K_{mean} = \frac{1}{r_7}\left\{\frac{\ln(r_5/r_4)}{k_4} + \frac{\ln(r_6/r_5)}{k_5} + \frac{\ln(r_7/r_6)}{k_6} + \frac{1}{hr_7}\right\}^{-1} \tag{1.10}$$

The total heat flux from the emitter, Q_{in}, is given by

$$Q_{in} = Q_{rad} + Q_{eE} + Q_{Cs} \quad . \tag{1.11}$$

Equilibrium at the emitter requires that Q_{FUEL} and Q_{in} are equal. The heat flux into the collector, Q_{out} is given by

$$Q_{out} = Q_{rad} + Q_{eC} + Q_{Cs} \quad . \tag{1.12}$$

Equilibrium at the collector requires that Q_{out} and Q_{NaK} are equal.

It can be seen from equations 1.3, 1.11 and 1.12 that at equilibrium the difference between Q_{TISA} and Q_{NaK} is equal to the difference between Q_{eE} and Q_{eC}, the output power flux, $J_{out}V_{out}$.

In the Ya-21u data there are reliable values for T_{NaK} at the inlet and outlet of the reactor core, as a function of q_{FUEL}. A plot of this data and the analytical expression used in the codes are shown in figure C1. This data was taken from run 8 of Ya-21u. The codes take T_{NaK} as the average of the inlet and outlet temperatures, a suitable value for a position halfway along the length of the TFE. The use of this T_{NaK} value as a boundary condition has enabled us to "terminate" the heat transfer calculations at the NaK channel. Firstly calculations are made of the temperatures and heat fluxes in the TFE under typical Ya-21u operating conditions, using EQ1D. The experimental q_{FUEL}/T_{NaK} calibrations for the reactor inlet and outlet are used to fix the average T_{NaK} for a given TISA power. The code is used to find the equilibrium conditions. These calculations give a value for Q_{out} at that q_{FUEL}. Since this value of Q_{out} depends on J_{out} (1.12), the calculated value of J_{out} must be similar to that when the data was recorded. The value of P_{Cs} used in the calculation is adjusted to achieve this agreement. Ya-21u has been run at relatively low output currents, where the electron heat transfer term is the order of 10% of the radiative term. EQ1D is run at values of q_{FUEL} in the range 1.0 - 3.5 kW (equivalent to a total reactor thermal power of 37 - 130 kW). It is then possible to produce a calibration of Q_{out} and T_{NaK}. This calibration is valid under a wide range of operating conditions, since T_{NaK} is a unique function of the heat flux into the NaK. However, a slightly different fit is used depending on whether electrode voltage drops are included in the calculation. This is because when the calibration is generated, the calculated J_{out}, and hence the value of Q_{out}, is dependent on the magnitude of the voltage drop. Due to the relatively small contribution of electron cooling to the total heat flux in these calculations, there is a very small difference between these two calibrations. Strictly speaking, the effect of NaK flow rate should be accounted for (equation A4), but this thermal resistance is insignificant in comparison with the other terms in equation 1.10. This new Q_{out} / T_{NaK} calibration is used in the more general calculations, performed using NAK1D. It is shown in figure C2, together with the analytical expression used in the codes.

1.2.2.1 Effective emissivity of inter-electrode gap

The effective emissivity of the inter-electrode gap, ε_{eff}, is defined by equation 1.2. The value used in these models is given by Nikolaev (1992) as

$$\varepsilon_{eff} = 0.142 + \left(1.26 \times 10^{-5} T_E\right). \tag{1.13}$$

In the heat transfer codes all the values of ε_{eff} used in a calculation can be multiplied by a scaling factor entered by the user.

1.2.3 Cesium pressure - reservoir temperature relationship

The relationship between P_{Cs} and the equivalent cesium reservoir temperature, T_R, needed to produce this pressure, is given by Hatsopoulos and Gyftopoulos (1973) as

$$P_{Cs} = 2.45 \times 10^{8} T_R^{-0.5} \exp\left(-\frac{8910}{T_R}\right). \tag{1.14}$$

In a TOPAZ-II reactor, the Cs supply is not a simple reservoir of the liquid metal, since this would require very precise temperature control to maintain a constant P_{Cs}. Despite this, the concept of equivalent reservoir temperature is still applicable in calculating electrode work functions.

1.2.4 I-V characteristics

The I-V characteristic code is central to both of the heat transfer models. It consists of separate models for the ignited (discharge) and unignited (diffusion) modes of TFE operation. Both of these models were originally developed by McVey (McVey and Rasor, Dahlberg *et. al.* 1994, Rasor Associates 1991), as TECMDL and UNIG respectively. The theory of both of these models will not be described further here. Both of these codes represent an improvement in accuracy over the original "phenomenological" model developed by Rasor (1982). Details of the I-V characteristic code are given in Section 3 of this report.

The present ignited mode code is based on TECMDL, with some changes to suit the needs of these calculations. The main difference is that both TECMDL and UNIG input a value for J_{out} and return the corresponding V_{out}. For the present work it was more convenient to input V_{out} and calculate J_{out}. In the ignited mode this has changed the order of some iterations in the calculation. No modifications have been made to the UNIG code, but an iterative routine has been added to precede it which allows the calculation of the current at the required voltage.

1.2.4.1 Work functions

The emitter work function (ϕ_E) used in these codes was taken from Hatsopoulos and Gyftopoulos (1973). It is shown in figure C3, together with the analytical expression used in the codes. The work function depends only on T_E/T_R and is only applicable to Cs on W. It was derived from measurements of work function as a function of Cs coverage. Since the thermionic emission process is strongly dependent on emitter work function, it is inevitable that some differences occur between experimental and calculated work function value, even for a "pristine" TFE. In the heat transfer codes all the values of ϕ_E used in a calculation can be multiplied by a scaling factor entered by the user.

The collector work function used is based on previous studies by other workers comparing calculations with experiment (McVey and Rasor, Dahlberg *et. al.* 1994). It has been found by these workers to give a better fit to experimental data than measurements made on individual materials outside of the TFE collector environment. It is applicable to collectors made from different metals. It is a function of T_C/T_R, and is shown in figure C4, together with the analytical expression used in the codes.

1.2.4.2 Voltage losses in electrodes

The option exists within all the programs to allow for voltage drops due to resistive losses in the emitter and the collector. The derivation of the following equations for voltage losses in the electrodes is given in Appendix B. Nikolaev *et. al.* (1991) gives the resistivities of the emitter (ρ_E) and the collector (ρ_C), in a TOPAZ-II TFE at typical operating temperatures as

$$\rho_E = \left(4.3\times10^{-8}T_E\right) - 2.3\times10^{-5} \quad (\Omega\ \text{cm}) \tag{1.15}$$

$$\rho_C = \left(2.8\times10^{-8}T_C\right) - 2.0\times10^{-6} \quad (\Omega\ \text{cm}) \tag{1.16}$$

For the active zone of one electrode, the voltage drop, V_{act} is given by

$$V_{act} = \frac{\rho(T)IX}{4A_{XC}}\ , \tag{1.17}$$

where $\rho(T)$ is the resistivity of the electrode at the temperature, T, of the active zone (emitter or collector), I is the current flowing from the TFE, X is half of the active zone length (15 cm in a TOPAZ II TFE) and A_{XC} is the cross sectional area of the electrode (calculated using the dimensions shown in figure 1.1).

For the inactive zone of one electrode, the voltage drop, V_{inact}, is given by

$$V_{inact} = \frac{I}{2A_{XC}}\left(\rho_H Y + \tfrac{1}{2}\dot{\rho}Y^2\right) \tag{1.18}$$

where ρ_H is the resistivity at the hot end of the inactive zone (i.e. at the emitter or collector temperature), Y is the length of the inactive zone on one side of the TFE (9.25 cm in a TOPAZ II TFE), and $\dot{\rho}$ is the resistivity gradient along the inactive zone, measured from the hot to the cold end. In the calculations the temperature of the cold end of both the emitter and the collector is taken to be equal to the NaK temperature. The total voltage loss is given by the sum of the active and inactive zone losses in the emitter and the collector.

References

Burdi, G. F. (1964) "SNAP Technology Handbook, Vol. 1: Liquid Metals," *NAA-SR-8617, Reactor Technology, TID-4500 (29th ed.)*, SNAP Reactors.

CRC Handbook of Chemistry and Physics (1976), CRC Press, Cleveland, OH.

Dahlberg, R. C., L. L. Begg, J. N. Smith, G. O. Fitzpatrick, D. T. Allen, G. L. Hatch, J. B. McVey, N. S. Rasor, D. P. Lieb and G. Miskolczy (1994) "Review of Thermionic Technology: 1983 to 1992," in "*A Critical Review of Space Nuclear Power and Propulsion 1984-1993,*" M. S. El-Genk, ed. AIP Press, New York p121.

Grigorieva, I. S. and E. Z. Melikhova (1991) "Handbook, Physical Constants," *Atomizdet,* Moscow.

Hatsopoulos, G. N. and E. P. Gyftopoulos (1973) "Thermionic Energy Conversion, Vol.1 Processes and Devices," MIT Press, Cambridge, MA.

Kreith, K. and W. Z. Black (1980) "Basic Heat Transfer," Harper and Row, New York.

McVey, J. B. and N. S. Rasor "The TECMDL Thermionic Converter Computer Model," Rasor Associates, Inc., San Jose, CA. See also Rasor documents E-563-002-A-063087 and E-563-004-C-082988.

Nikolaev, Y. V. et. al. (1991) "Thermionic Fuel Element of Power Plant TOPAZ-II," *Report JV "INERTEK"*, Moscow.

Nikolaev, Y. V., V. Androsov, V. Vybyvanetz, A. Grigoriev, B. Igumnov, O. Izhvanov, V. Modin, A. Olchovski, V. Osmachkin and E. Chadrin (1992) "Control Test of Power Plant TOPAZ-II Single Cell TFE at The Rig," *Report JV "INERTEK"*, Moscow.

Paramonov, D. V. and M. S. El-Genk (1994) "Steady-State and Transient Analyses of the Topaz-II Space Nuclear Power System," *UNM Report No. UNM-ISNPS-3-1994*, Albuquerque, NM.

Rasor, N. S. (1982) "Thermionic Energy Conversion," *Applied Atomic Collision Physics*, 5: 170.

Rasor Associates, Inc. (1991) "Preliminary Technical Report: UNIG Unignited Mode Thermionic Converter Model," *Rasor Associates, Inc. Report* NSR-53-91-0134, San Jose, CA.

Schmidt, G., S. Wold, J. M. Taylor and F. J. Wyant (1995) "TOPAZ-II Ya-21u System Test Report," *Topaz International Program Report*, Albuquerque, NM. To be published

Steppenov, B. S., N. N. Ponomarev-Stepnoi, V. P. Nikitin and Y. V. Nikolaev (1991) "NPS TOPAZ-II Description," *Report JV "INERTEK"*, Moscow.

Wold, S., R. Burson, and T. Way (1994) "American Testing of the Topaz-II: Results of the Ya-21 Thermal Tests", in *Proc. 11th Symposium on Space Nuclear Power and Propulsion*, M. S. El-Genk and M. D. Hoover, eds., American Institute of Physics, New York, AIP Conference Proc. No. 301 p813.

U.S. Topaz-II Flight Safety Team (1992) "NEP Space Test Program Preliminary Nuclear Safety Assessment," *Topaz International Program Report*, Albuquerque, NM.

Appendix A - Calculation of convective heat transfer to NaK coolant

For a cylindrical geometry, the convective heat transfer coefficient, h, between concentric annuli is given by (Burdi 1964)

$$h = \frac{k_{NaK}}{D}\left[A + BPe^{C}\right] \quad . \tag{A1}$$

k_{NaK} is thermal conductivity of the NaK coolant, a function of T_{NaK}. A plot of k_{NaK} as a function of temperature, and the analytical expression used in the codes is shown in figure C8 (Paramonov and El-Genk 1994). D is a characteristic distance given by (figure 1.1)

$$D = 2\left(r_8 - r_7\right) \quad . \tag{A2}$$

Pe is the Peclet number for the NaK coolant, defined as (Kreith and Black 1980)

$$Pe = Re.Pr \quad , \tag{A3}$$

where Re is the Reynolds number and Pr is the Prandtl number of the NaK.

Pe can be expressed as (Kreith and Black 1980)

$$Pe = \frac{\dot{m}Dc_p}{k_{NaK}A_{NaK}} \quad , \tag{A4}$$

where $\dot{m}$ is the NaK mass flow rate through the TFE, c_p is the NaK specific heat capacity and A_{NaK} is the cross-sectional area of the NaK channel, given by

$$A_{NaK} = \pi\left(r_8^2 - r_7^2\right) \quad . \tag{A5}$$

A plot of c_p as a function of temperature, and the analytical expression used in the codes are shown in figure C9 (Paramonov and El-Genk 1994).

Defining γ as the ratio r_8/r_7, the coefficients A, B, and C are given by (Burdi 1964)

$$A = 4.63 + 0.686\gamma \quad , \tag{A6}$$

$$B = 0.215 + 4.3\times10^{-5}\gamma \quad , \tag{A7}$$

$$C = 0.752 + 0.01657\gamma - 8.83\times10^{-4}\gamma^{2} \quad . \tag{A8}$$

Appendix B - Calculation of voltage losses in electrodes

A schematic of the current path through a single TOPAZ-II TFE is shown in figure B1. I is the total current through the TFE. There are current connections at both ends of the emitter and collector. It has been assumed that half of the total current flows through each electrode connection. The current density is taken to be uniform across the active zone of the TFE, and zero elsewhere.

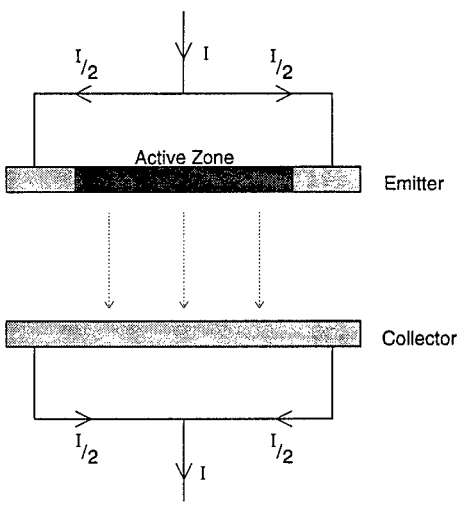

Figure B1: Current path through a TOPAZ-II TFE.

The assumed temperature of each electrode as a function of distance along the electrode is shown in figure B2.

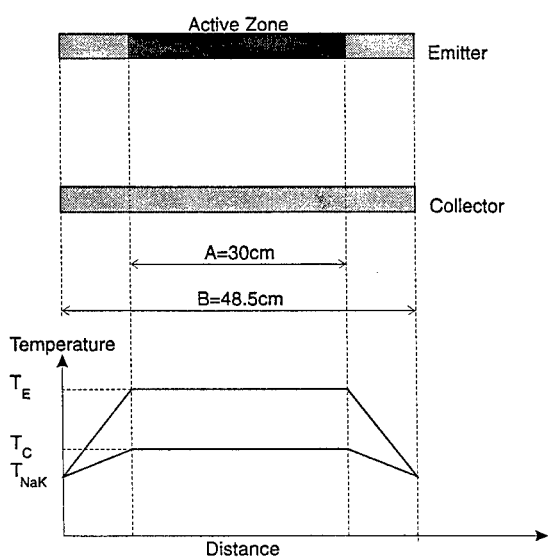

Figure B2: Emitter and collector temperature profiles used in calculations.

The variation of electrical resistivity with position along the electrodes is shown in figure B3, together with dimensions used in the following derivations. The resistivity at any point on either electrode is calculated using equations 1.15 and 1.16. Equation 1.15 is used for the active zone of the emitter (point Q). Equation 1.16 is used for the whole length of the collector and also the cold ends of the emitter (point R). Resistivities at intermediate points on the inactive zone of the emitter (points Q to R) are calculated using an extrapolation between the end of the active zone and the cold end of the emitter. In using the collector equation for the cold end of the emitter, the fact that the emitter and collector are made of different materials is neglected. However, equations 1.15 and 1.16 are fits to experimental values of resistivity at typical emitter and collector temperatures, so it is not valid to use the emitter equation at the NaK temperature. The aim here is to approximate the resistivity of the inactive zone rather than accurately model its resistivity.

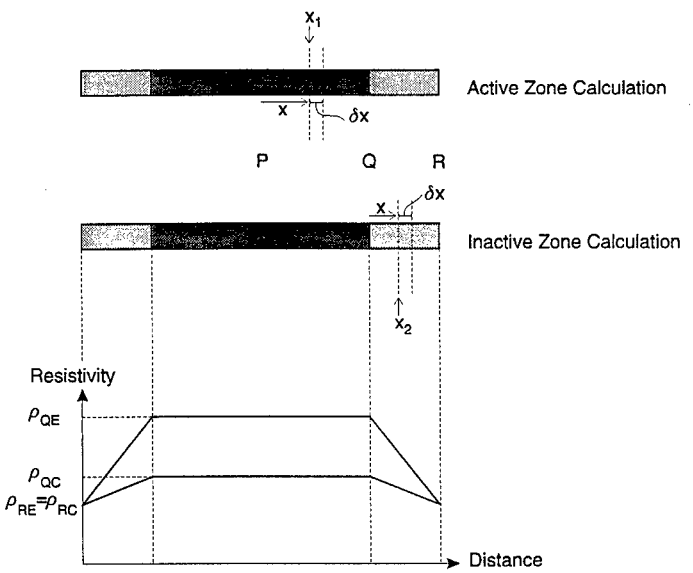

Figure B3: Emitter and collector resistivity profiles used in calculations.

Active zone losses

At a general point X_1 along the length of the TFE, the current flowing, i, (in either electrode) is given by

$$i = \frac{I}{2}\frac{x}{X}\ , \qquad \text{(B1)}$$

where x is the distance from the centre of the TFE (point P) and X is half the length of the active zone (15 cm). The current flowing along the electrode varies along the active zone, as electrons are moving across the gap along the active zone. At either end of the active zone, x = X and the current = I/2, as shown in figure B1.

Considering a small length δx of one electrode at X_1, the resistance δR of that element is given by

$$\delta R = \frac{\rho(T)\delta x}{A_{XC}} \quad , \tag{B2}$$

where A_{XC} is the cross sectional area of that electrode. The resistivity of the electrode, ρ(T) is constant along the active zone of either electrode, since the temperature is assumed to be constant. The voltage drop, δV, due to this resistance is given by the product of resistance and current at that point,

$$\delta V = \frac{Ix}{2X}\frac{\rho(T)\delta x}{A_{XC}} \quad . \tag{B3}$$

The total V drop from P to Q, in either electrode is given by

$$V_{act} = \int_0^X \frac{Ix}{2X}\frac{\rho(T)}{A_{XC}}dx \tag{B4}$$

This gives the drop in either active zone as

$$V_{act} = \frac{\rho(T)}{4A_{XC}}IX \quad . \tag{B5}$$

Inactive zone losses

In this region the current is constant at a value of I/2 but the resistivity changes along the length due to the change in temperature. Point Q (figure B3) is now considered as the origin of x values, for simplicity. The electrode resistivity at Q is calculated from equation 1.15 or 1.16 as ρ_Q and that at R is calculated from equation 1.16 as ρ_R. The value of resistivity at any point X_2 is given by

$$\rho(x) = \rho_Q + \dot{\rho}x \quad , \tag{B6}$$

where $\dot{\rho}$ is the resistivity gradient from Q to R on the emitter, given by

$$\dot{\rho} = \frac{\rho_R - \rho_Q}{Y} \quad (<0). \tag{B7}$$

Y is the distance from the end of the active zone to the end of the electrode (9.25 cm).

The resistance δR of element δx on the inactive zone is given by

$$\delta R = \frac{\rho(x)\delta x}{A_{XC}} \quad . \tag{B8}$$

The corresponding voltage drop δV is given by

$$\delta V = \frac{I}{2}\frac{\rho(x)\delta x}{A_{XC}} \quad . \tag{B9}$$

By integrating equation B9 and substituting equation B6, the total voltage drop V_{inact} from Q to R, along the inactive zone of either electrode is found to be

$$V_{inact} = \int_0^Y \frac{I}{2}\frac{\rho(x)}{A_{XC}}dx = \frac{I}{2A_{XC}}\int_0^Y (\rho_Q + \dot{\rho}x)dx \quad . \tag{B10}$$

$$V_{inact} = \frac{I}{2A_{XC}}\left[\rho_Q Y + \tfrac{1}{2}\dot{\rho}Y^2\right] \quad . \tag{B11}$$

Appendix C - Data used in calculations

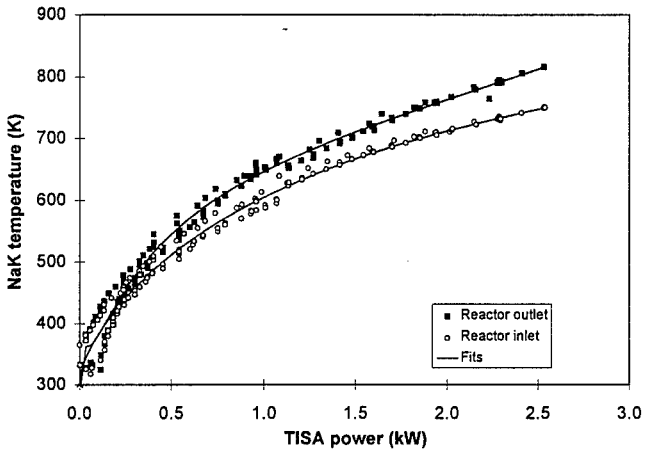

Figure C1: NaK temperature as a fuction of TISA power, q_{FUEL}.

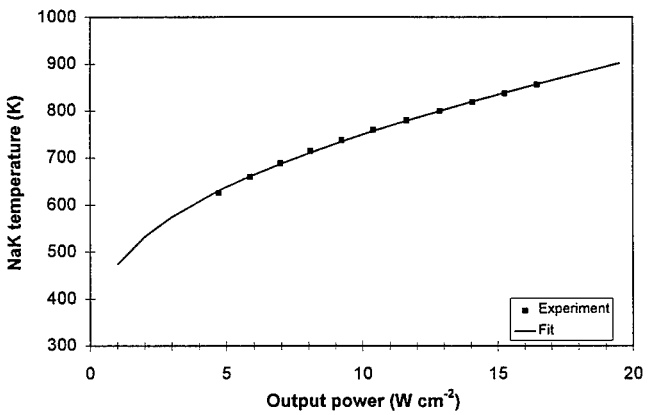

Figure C2: NaK temperature as a function of TFE thermal output power Q_{out}.

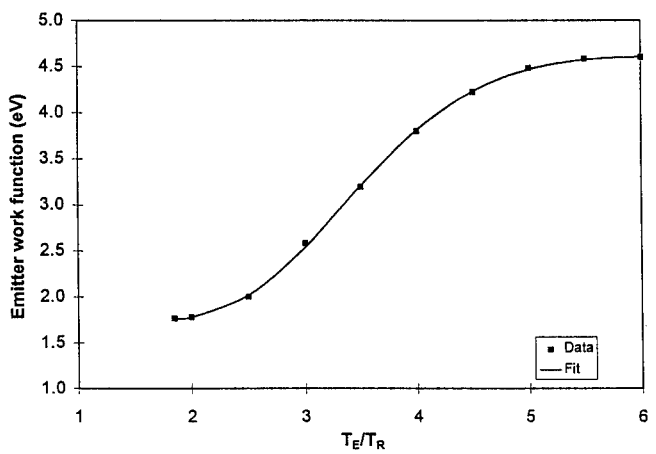

Figure C3: Emitter work function, ϕ_E, as a function of T_E/T_R.

T_{NaK} at the reactor outlet is fitted as

$$T_{NaK} = A + Bx + Cx^2 + Dx^3 + Ex^4 + Fx^5 + Gx^6,$$
$$x = \ln(q_{FUEL})$$

A = 646.08602
B = 150.47498
C = 12.247623
D = 12.042109
E = 10.590804
F = 2.4922993
G = 0.1794822.

T_{NaK} at the reactor inlet is fitted as

$$T_{NaK} = A + Bq_{FUEL} + Cxq_{FUEL} + Dq_{FUEL}^{1.5} + E\,x/q_{FUEL}^2$$

A = 314.80292
B = 179.19923
C = -197.56921
D = 110.60518
E = $-7.0386418 \times 10^{-16}$.

$$T_{NaK} = \left(A + B\ln Q_{out}\right)^{-1},$$

	With electrode losses	Without electrode losses
A	2.1088286×10^{-3}	$-3.3650990 \times 10^{-4}$
B	2.1084566×10^{-3}	$-3.3642567 \times 10^{-4}$

$$\phi_E = \frac{A + C\ln(T_E/T_R) + E\left(\ln(T_E/T_R)\right)^2}{1 + B\ln(T_E/T_R) + D\left(\ln(T_E/T_R)\right)^2}$$

A = 1.9480958
B = -1.2642181
C = -2.8772769
D = 0.48526772
E = 1.4189757.

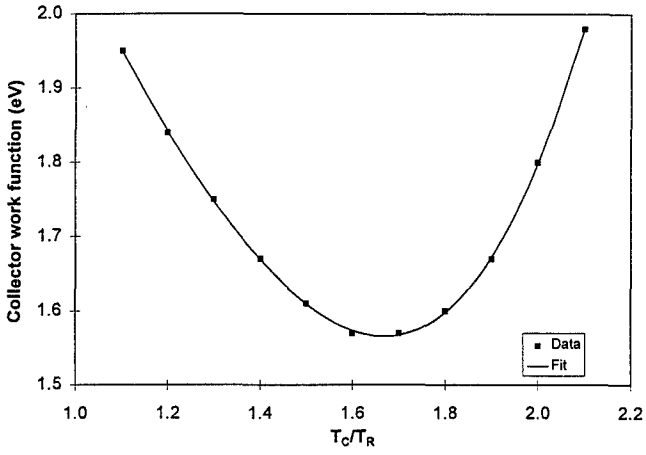

Figure C4: Collector work function, ϕ_C, as a function of T_C/T_R.

$$\phi_C = A + B(T_C/T_R)^{1.5} + C\sqrt{T_C/T_R} + D\exp(-T_C/T_R)$$

A = 214.99825
B = 20.424012
C = -176.92743
D = -153.3579.

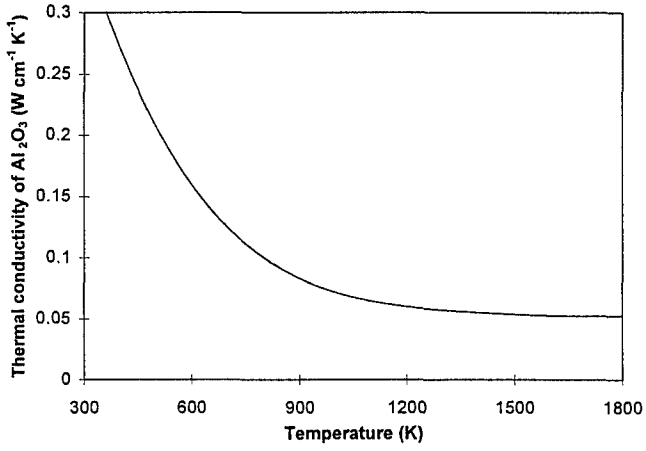

Figure C5: Thermal conductivity of Al_2O_3, k_4, as a function of temperature.

$$k_4 = A + BT + CT^2 + DT^3 + ET^4$$

A = 0.749
B = -1.78 x 10^{-3}
C = 1.75 x 10^{-6}
D = -7.78 x 10^{-10}
E = 1.31 x 10^{-13}

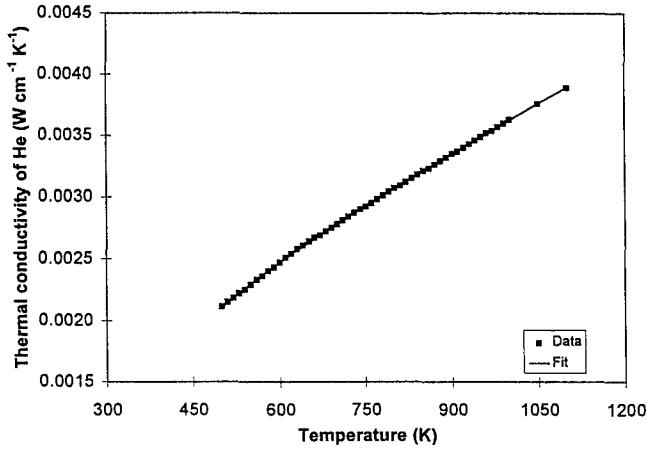

Figure C6: Thermal conductivity of He, k_5, as a function of temperature.

$$k_5 = A + BT + CT^2 + DT^{2.5} + ET^3$$

A = -4.1509458 x 10^{-3}
B = 3.1161155 x 10^{-5}
C = -9.7059484 x 10^{-8}
D = 3.498383 x 10^{-9}
E = -3.6954186 x 10^{-11}

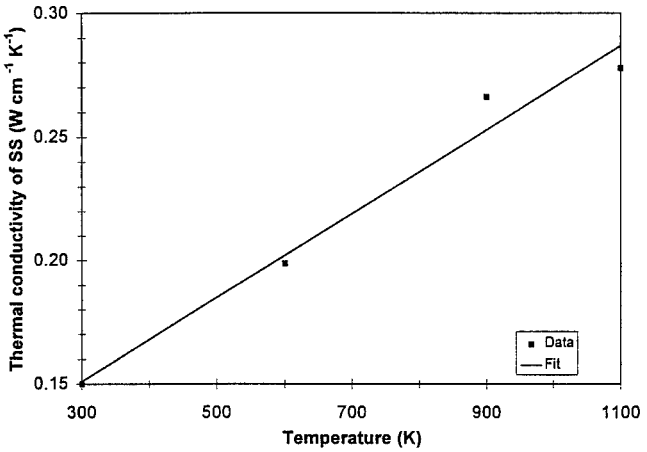

$k_6 = A + BT$

A = 0.10
B = 1.7×10^{-4}

Figure C7: Thermal conductivity of stainless steel, k_6, as a function of temperature.

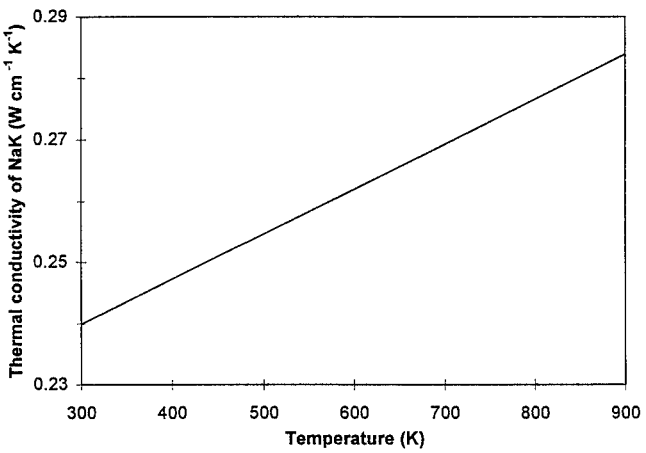

$k_7 = A + BT$

A = 7.33×10^{-5}
B = 0.218

Figure C8: Thermal conductivity of NaK, k_7, as a function of temperature.

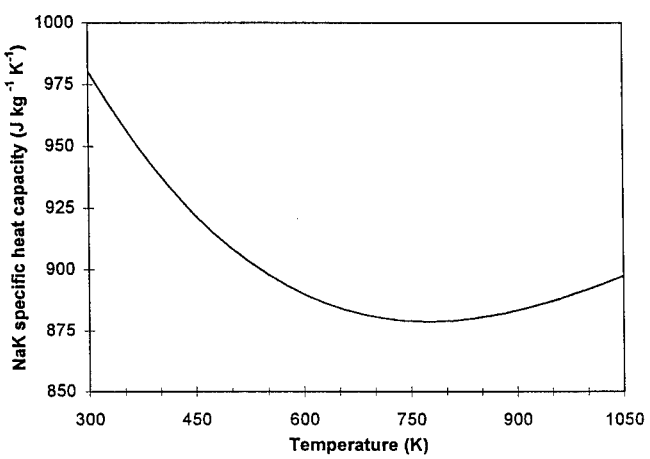

$c_p = A + BT + CT^2 + DT^3$

A = 1.20
B = -9.96×10^{-4}
C = 9.66×10^{-7}
D = -2.78×10^{-10}

Figure C9: Specific heat capacity of NaK, c_p, as a function of temperature.

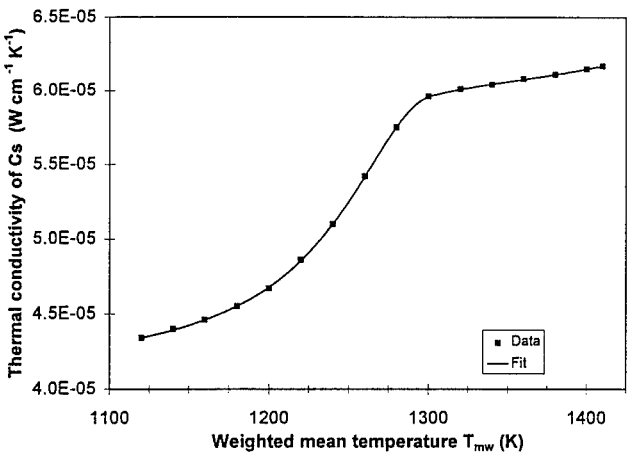

Figure C10: Thermal conductivity of Cs vapor, λ_{mw}, as a function of weighted mean temperature T_{mw}.

$\underline{T_{mw} < 1120\ K}$

$\lambda_{mw} = 4.343 \times 10^{-5}\ W\ cm^{-1}\ K^{-1}$

$\underline{1120 \leq T_{mw} \leq 1300\ K}$

$$\lambda_{mw} = 10^{-5}\left(A + \frac{B}{\left(1 + \left((T_{mw} - C)/D\right)^2\right)} \right)$$

A = 4.1135398
B = 1.8563891
C = 1305.3302
D = 69.608997

$\underline{1300 < T_{mw} \leq 1410\ K}$

$$\lambda_{mw} = 10^{-5}\left(\frac{1}{A + B/\ln t_{mw} + C \ln t_{mw}/t_{mw}^{\ 2}} \right)$$

$t_{mw}=T_{mw}/1000$
A = -0.69949787
B = 0.077973985
C = 3.6720771

$\underline{T_{mw} > 1410\ K}$

$\lambda_{mw} = 6.171 \times 10^{-5}\ W\ cm^{-1}\ K^{-1}$

Section 2 - Applications

2.1. Introduction

The 1-D thermal models EQ1D and NAK1D have been used to analyse data recorded from the TOPAZ II reactor Ya-21u. As has been previously mentioned, this reactor has been subjected to a rigourous series of tests, both in Russia and the US. Leaks in several of the TFEs have resulted in exposure of the TFEs to air on several occasions when the reactor has been cold. As a result of these extreme conditions changes in the performance of the reactor have occurred over time. In the following analysis the model has been used to examine the effects of changes to various operating parameters of the reactor to help determine the effects of extended testing.

2.2. Data analysis

2.2.1 Experimental data

Data has been taken from 4 runs of Ya-21u. These are :-

Run	Dates
3	12/10/93 - 12/23/93
6	4/1/94 - 4/22/94
7	8/1/94 - 8/8/94
8	8/10/94 - 8/17/94

All these runs are before the shake and vibration test, which was performed immediately following run 8. Data from after the shake and vibration test has not been included in this report as it shows much larger changes in reactor output, which may have causes other than those considered here. In run 6 the thermal shield to the radiator of the reactor was removed. The purpose of this shield is to increase the NaK coolant temperature (T_{NaK}) in the reactor during electrical testing in vacuum. This maintains T_{NaK} at a more realistic operating temperature during thermal vacuum testing. The shield was present during runs 3, 7 and 8. Runs 7 and 8 were intended to be a single run, but an emergency condition forced a shutdown of the reactor at the end of run 7. Hence data from run 7 is only available for a few operating conditions. Air intrusions into the TFE inter-electrode gaps over the time-span of this data are known to have occurred prior to run 3 and between runs 3 and 6.

Figure 2.1 shows reactor I-V characteristics recorded at nominal conditions of thermal power = 85 kW and 95 kW, P_{Cs} = 0.6 Torr and 0.7 Torr. The data sets shown with solid connecting lines have been fitted in the calculations described below. The following conclusions can be drawn. There has been a gradual decrease in output from run 3 to run 8. In figure 2.1a (85 kW, 0.6 Torr) where data from run 7 is present, it shows a good agreement with run 6 and a less good agreement with run 8. This shows that a significant change occurred between runs 7 and 8. This

can most likely be attributed to the emergency shutdown and corresponding rapid cool down of the reactor at the end of run 7. The data from run 6 fits well with the trends shown by the other runs, suggesting that removal of the thermal shield did not have a large effect on the reactor output power under these operating conditions. The data from run 8 shows a significantly larger incremental decrease in output than is seen between the other runs, and also a steeper I-V characteristic. This may indicate that the reactor has changed to operating in the unignited (diffusion) mode over some of the voltage range. In addition the I-V characteristics in figures 2.1b and 2.1d (95 kW, 0.6 and 0.7 Torr) appear to show a change in gradient at around 21 V which may correspond to a transition between the unignited and ignited modes. It should also be noted that in figure 2.1a where two data sets are shown from run 3, there is a significant difference between the two data sets. The cause of this is unknown, but it may be due to the air intrusion which occurred prior to this run. The data set recorded on 12/20/93 has been fitted in the following calculations, as this is more consistent with the data available in the runs where only one optimization was performed.

2.2.2 Data fitting

Preliminary analysis of the data shown in figure 2.1 indicates that using the nominal values for all parameters in NAK1D produces current densities around 40% higher than the measured values. Inaccuracies in the TECMDL code, on which the I-V characteristic part of the current model is based, are not enough to explain this discrepancy. Precise comparisons of TECMDL with experimental data are difficult due to the difficulty in accurately measuring experimental parameters, such as emitter temperature and emitter and collector work functions, which are required in the calculation. However existing comparisons (McVey and Rasor, Dahlberg *et. al.* 1994) indicate errors generally not greater than 10% between experimental data and TECMDL. The temperatures of the electrodes, which are used in calculating the I-V characteristic, are determined by the heat transfer part of the model. The heat transfer codes use published values for the thermal conductivities of the necessary components. Whilst there may be some deviations from these values, they would be unlikely to produce the differences between experiment and calculation observed for the Ya-21u data. The only "heat transfer" term which has been allowed to vary in this work is the effective emissivity, ε_{eff}, of the inter-electrode gap. This is a combination of the emissivities of the emitter and collector, and determines the net radiative heat transfer between the emitter and the collector. The emissivity of a surface is strongly dependent on the surface finish and is likely to have been affected by the long test history of Ya-21u. The effective emissivity has been varied using a multiplying factor which scales the default value.

In fitting data from run 6, the option in NAK1D to change T_{NaK} was used. Experimental values of T_{NaK} at the reactor outlet in run 6 were 460 K and 484 K, at 85 kW and 95 kW respectively. In runs 3 and 8 the T_{NaK} values at these same thermal powers were 519 K and 543 K respectively. Hence the change in T_{NaK} from "normal" conditions with the radiator shield in place was -59 K.

It has long been suspected that the Cs throttle valve on Ya-21u does not accurately supply the nominal Cs pressures indicated by the valve position. This suspicion is based on the observed reactor output, particularly discrepancies between the theoretical and actual optimum Cs

pressures for a given thermal power. Hence the Cs pressure (P_{Cs}) has been varied in these calculations to fit the calculated output to the experimental data. The primary effect of this P_{Cs} change in terms of output current density (J_{out}) is on the emitter work function (ϕ_E), via the variation in Cs reservoir temperature (see figure C3). The collector shows a much slower variation in work function (ϕ_C) with P_{Cs} under typical operating conditions (figure C4).

For a given reactor thermal power, the electrical output power increases with P_{Cs} at low P_{Cs}, passes through a maximum and then falls more slowly as P_{Cs} is further increased. The value of the optimum P_{Cs} increases as the thermal power increases. In Ya-21u experimental values of J_{out} at given output volts (V_{out}) have been lower than expected. The value used for P_{Cs} in the model can either be decreased or increased to fit the experimental data. Fitting the 95 kW, 0.6 Torr I-V characteristic from run 3 with a P_{Cs} value higher than the nominal value shows that a P_{Cs} value of 4.0 Torr fits the value of J_{out} at 24 V and produces an I-V characteristic of similar gradient to the experimental data. However, if the NaK temperature used in the model is lowered by 59 K, J_{out} is seen to decrease by around 24%. This is much larger than the change which was observed to occur in run 6. The possibility that the Cs system is producing much higher P_{Cs} values than expected can effectively be ruled out by this information. In the following work, where P_{Cs} values are changed to fit the data, it has been assumed that experimental P_{Cs} values are lower than the nominal values.

The second variable in this work has been the emitter work function, ϕ_E, since this may have changed from its nominal temperature dependence by repeated testing. Variations in ϕ_E have been simulated by varying a multiplying factor which directly scales the whole of the emitter Rasor plot by a constant factor.

The final variable has been the value of ε_{eff} in the inter-electrode gap, which may have also changed from its original value after extended testing. Variations in ε_{eff} have been simulated by varying a multiplying factor which directly scales ε_{eff} as given in equation 1.13 by a constant factor.

Individual I-V characteristics were fitted using the value of J_{out} at the nearest experimental data point to V_{out} = 24 V. The remaining data points on the I-V characteristic were calculated by changing only the TFE output volts. P_{Cs}, the ϕ_E multiplier and the ε_{eff} multiplier were left the same as that used at 24 V. Table 2.1 shows the results of fitting the indicated data sets by modifying P_{Cs} to the value shown in column 4 from its nominal value (column 3). The fits produced are shown in figures 2.2 and 2.3. ϕ_E was as shown in figure C3. Column 5 shows the calculated value of ϕ_E at 24 V at the fitted P_{Cs} value. ϕ_E varies by typically 0.04 eV between the maximum and minimum voltages on the I-V characteristics. This is due to variations in the emitter temperature (T_E) as a result of changes in output current and therefore electron cooling. Column 6 shows the emitter work function which would have been calculated using the nominal operating P_{Cs}. Column 7 shows ε_{eff} for the inter-electrode gap, calculated from equation 1.13.

Run	TISA power (kW)	Nominal P_{Cs} (Torr)	P_{Cs} used (Torr)	ϕ_E (eV)	Nominal ϕ_E (eV)	ε_{eff}
3	85	0.6	0.37	3.129	2.874	0.1645
6	85	0.6	0.37	3.125	↓	0.1645
8	85	0.6	0.33	3.190	↓	0.1646
3	85	0.7	0.37	3.129	2.832	0.1645
3	95	0.6	0.46	3.161	2.978	0.1649
6	95	0.6	0.45	3.170	↓	0.1649
8	95	0.6	0.43	3.203	↓	0.1650
3	95	0.7	0.46	3.162	2.891	0.1649

Table 2.1 : Cs pressure values required to fit experimental I-V characteristics.

Table 2.2 shows the results of fitting the same data sets using the nominal value of P_{Cs} and modifying ϕ_E from its nominal value. This modification was achieved by multiplying the value produced by the emitter Rasor plot in figure C3 by the factor shown in column 4. Column 5 shows the calculated value of ϕ_E at 24 V. This again varies by typically 0.015 eV between the maximum and minimum voltages fitted. The fits produced are shown in figures 2.4 and 2.5. The output current was again fitted at 24 V.

Run	TISA power (kW)	Nominal P_{Cs} (Torr)	ϕ_E multiplier	ϕ_E (eV)	Nominal ϕ_E (eV)	ε_{eff}
3	85	0.6	1.044	3.108	2.874	0.1644
6	85	0.6	1.045	3.114	↓	0.1644
8	85	0.6	1.057	3.178	↓	0.1645
3	85	0.7	1.059	3.104	2.832	0.1644
3	95	0.6	1.024	3.151	2.978	0.1649
6	95	0.6	1.026	3.161	↓	0.1649
8	95	0.6	1.031	3.196	↓	0.1650
3	95	0.7	1.039	3.149	2.891	0.1649

Table 2.2 : Required emitter work function multiplier to fit experimental I-V characteristics.

Table 2.3 shows the effect of fitting the data from run 3 at 85, 95 kW, 0.6, 0.7 Torr by scaling the value of ε_{eff} by the values shown in column 4. This produce the ε_{eff} values shown in column 5. P_{Cs} and ϕ_E were left at their nominal values. However, ϕ_E was different to the nominal values shown above, since the increase in the radiative heat flux across the inter-electrode gap results in lower T_E values and therefore different values of ϕ_E. The fits produced are shown in figure 2.6. Since this method of fitting I-V characteristics did not produce as good an agreement between

experiment and fit as the previous methods, only the data sets produced in run 3 were fitted in this way. The changes in gradient in the fitted I-V characteristics are caused by a transition from the unignited mode to the ignited mode of operation.

Run	TISA power (kW)	Nominal P_{Cs} (Torr)	ε_{eff} multiplier	ε_{eff}	ϕ_E (eV)
3	85	0.6	1.21	0.1978	2.791
3	85	0.7	1.22	0.1994	2.746
3	95	0.6	1.34	0.2191	2.793
3	95	0.7	1.34	0.2191	2.752

Table 2.3: Required effective emissivity multiplier to fit experimental I-V characteristics.

2.3 Discussion

The following observations can be made:-

1. Tables 2.1 and 2.2 show that similar values of ϕ_E are obtained in fitting the experimental data, whether the data is fitted by changing P_{Cs} or by scaling ϕ_E. This is to be expected, since the main effect of a change in P_{Cs} in I-V characteristic calculations is to change the electrode work functions.

2. For a given P_{Cs}, different factors are required to scale ϕ_E at 85 and 95 kW. This implies that ϕ_E has degraded from its nominal Rasor plot, and cannot be described by uniform scaling of that plot. A smaller scaling factor is used at 95 kW, where T_E and therefore ϕ_E are higher. This means that the dependence of ϕ_E on T_E is not as strong as that in the emitter Rasor plot. This may be expected for a surface which has undergone long-term changes during the lifetime of the reactor.

3. The same P_{Cs} cannot be used to fit both 85 and 95 kW data at either 0.6 or 0.7 Torr. Unless the Cs throttle valve position cannot be accurately reproduced, the same P_{Cs} values should be produced at different thermal powers. If the problem is not caused by valve positioning, this observation again suggests that ϕ_E cannot be described by the existing Rasor plot. It is unlikely that if there was a problem with reproducibility in valve positioning, that the same trends would have been produced in the different runs discussed here. Even if ϕ_E is no longer described by the nominal Rasor plot, it is still also possible that the Cs system is not producing the nominal values of P_{Cs}. These two effects cannot be separated using the existing data.

4. There is less change in the I-V characteristic than expected, when P_{Cs} is changed from 0.6 to 0.7 Torr at either 85 or 95 kW. J_{out} at 24 V can be fitted with the same value of P_{Cs} within 0.01 Torr, or with a very similar value of ϕ_E. This suggests that either the Cs valve is not producing a significant change in P_{Cs} or that ϕ_E has less dependence on P_{Cs} than in the nominal Rasor plot.

5. The calculated I-V characteristics are too shallow in runs 3 and 8, too steep in run 6, when fitted by changing P_{Cs} or the ϕ_E multiplier. Once J_{out} is fitted at 24 V, the variation of ϕ_E as a function of the change in T_E along the I-V characteristic is assumed to obey the emitter Rasor plot shown in figure C3. Based on the points made above, this may not be a valid assumption, and may explain the discrepancies in I-V characteristic gradient. The magnitude of the difference in T_E along the I-V characteristic is similar in all runs, so another explanation is needed to explain the different trend seen in run 6. It may be that since the collector temperature is now also ~ 60 K lower in run 6 than in the other runs, that discrepancies from the collector Rasor plot (figure C4) are also being observed.

6. When J_{out} was fitted using the ε_{eff} multiplier, the I-V characteristics produced were much too steep. This suggests that the changes in reactor output cannot be explained by changes in ε_{eff} alone. In any case, it is unlikely that a change in ε_{eff} would occur without changes in the other parameters fitted. Since the fits produced by changing P_{Cs} or the ϕ_E multiplier produce slightly too low a gradient (point 5), it may be that some changes in ε_{eff} from the nominal value are also shown in this data.

7. The emitter Rasor plot used may itself have some "systematic" deviation from the true cesiated plot used. For example, another Rasor plot for Cs on tungsten in given by Rasor (1982). This shows deviations of up to 0.2 eV from the plot used in this work, at values of T_E/T_R typical of TOPAZ-II operating conditions. An error of this kind would be shown by the constant need for a ϕ_E multiplying factor. Even if this kind of error was present in these calculations, the values of ϕ_E required to fit the experimental data still cannot be described by a single Rasor plot.

2.4 Summary

The experimental data presented above suggests that the nominal emitter Rasor plot (figure C3) was not adhered to by the TOPAZ-II TFEs during runs 3 to 8. In particular, the reactor output is not as sensitive to changes in emitter temperature or cesium pressure as predicted by the Rasor plot for Cs on tungsten. It has long been suspected that the Cs valve was not producing the correct cesium pressures during these runs. This observation may be explained entirely by the deviation from the Rasor plot or there may be discrepancies in the reactor output caused by both work function changes and errors in cesium pressure caused by the cesium throttle valve. There may also be some changes in the effective emissivity of the inter-electrode gap from the nominal values, but the discrepancies in reactor output cannot be explained by this effect alone.

The absence of the radiator thermal shield in run 6 did not produce a large change in output power. This implies that the Cs pressure supplied by the reservoir is not significantly higher than the nominal value.

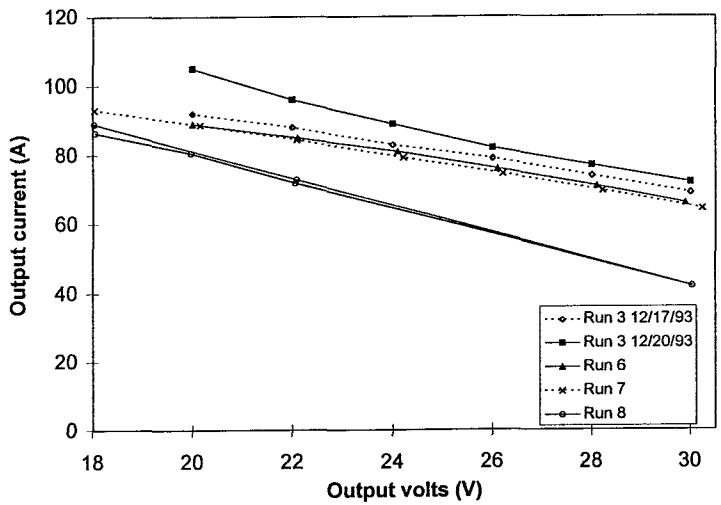

Figure 2.1a : 85 kW 0.6 Torr

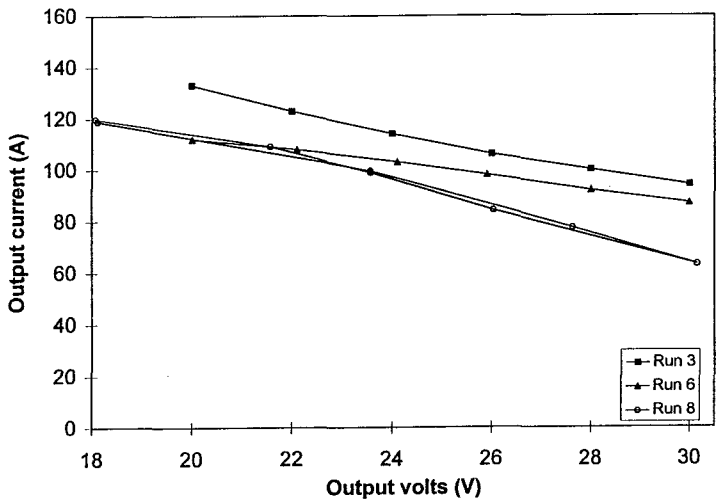

Figure 2.1b: 95 kW 0.6 Torr

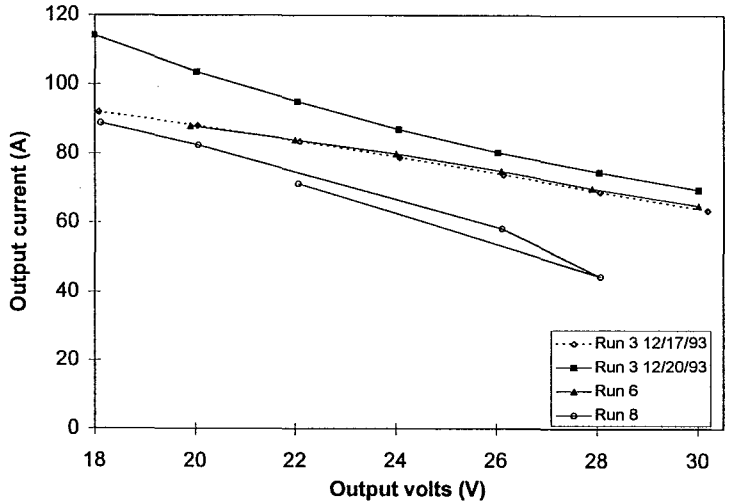

Figure 2.1c : 85 kW 0.7 Torr

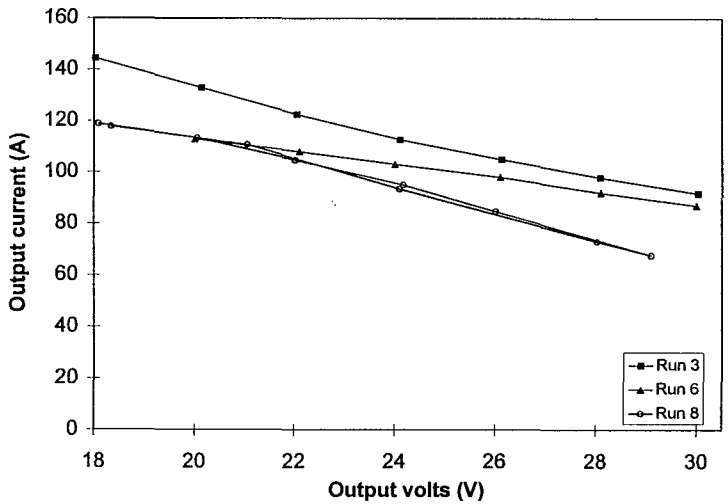

Figure 2.1d : 95 kW 0.7 Torr

Figure 2.1: Experimental I-V characteristics from runs 3, 6, 7 and 8

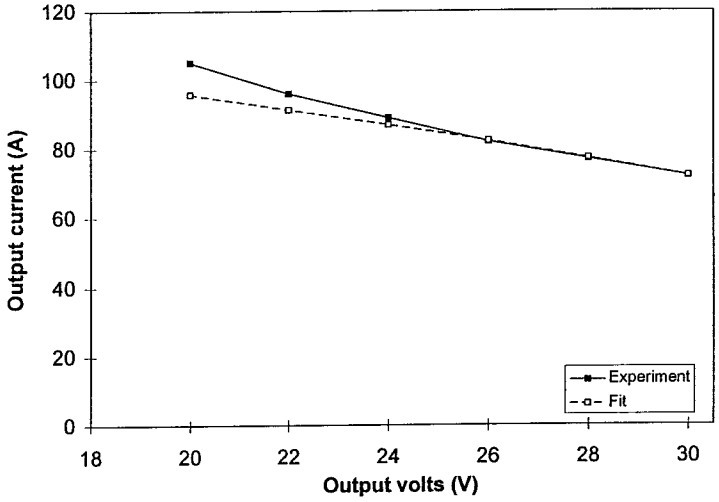

Figure 2.2a : Run 3, nominal 0.6 Torr, fitted as 0.37 Torr

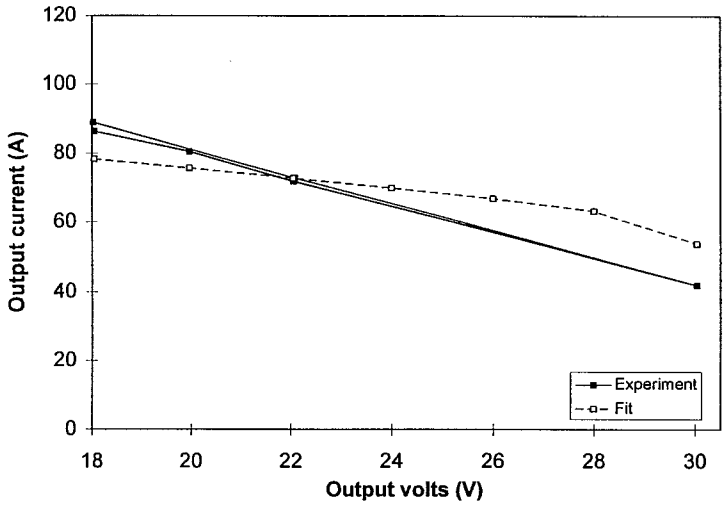

Figure 2.2c : Run 8, nominal 0.6 Torr, fitted as 0.33 Torr

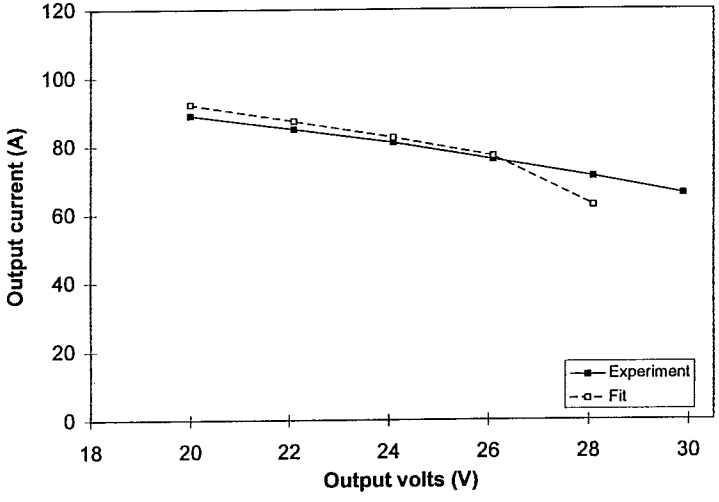

Figure 2.2b : Run 6, nominal 0.6 Torr, fitted as 0.37 Torr

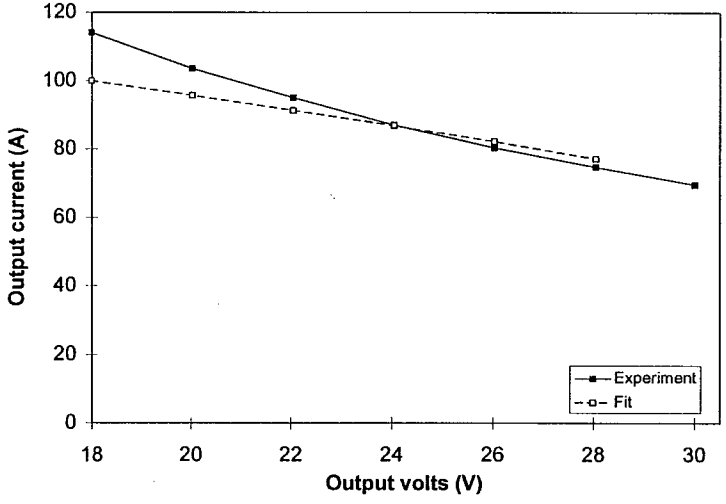

Figure 2.2d : Run 3, nominal 0.7 Torr, fitted as 0.37 Torr

Figure 2.2 : Thermal power = 85 kW, fitted by modifying Cs pressure

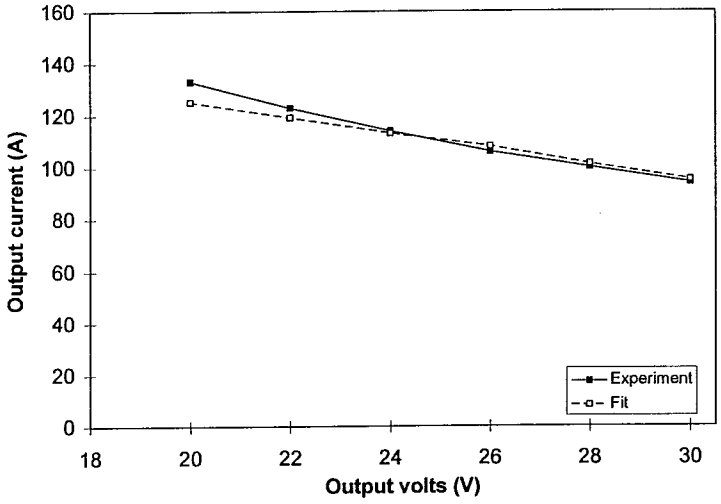

Figure 2.3a : Run 3, nominal 0.6 Torr, fitted as 0.46 Torr

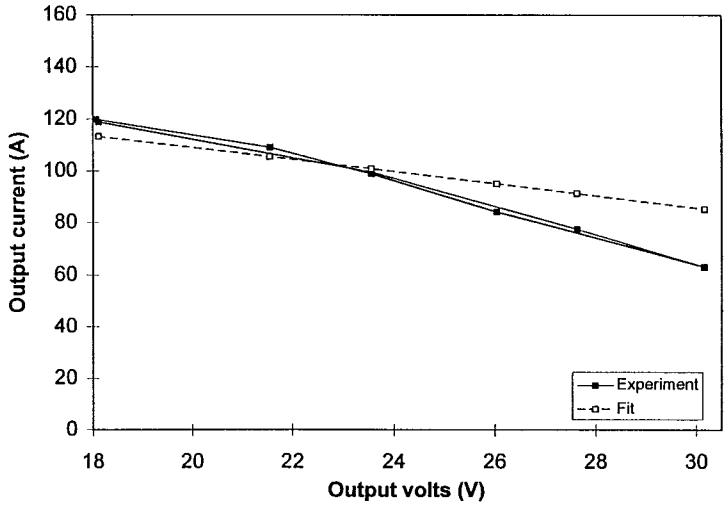

Figure 2.3c : Run 8, nominal 0.6 Torr, fitted as 0.43 Torr

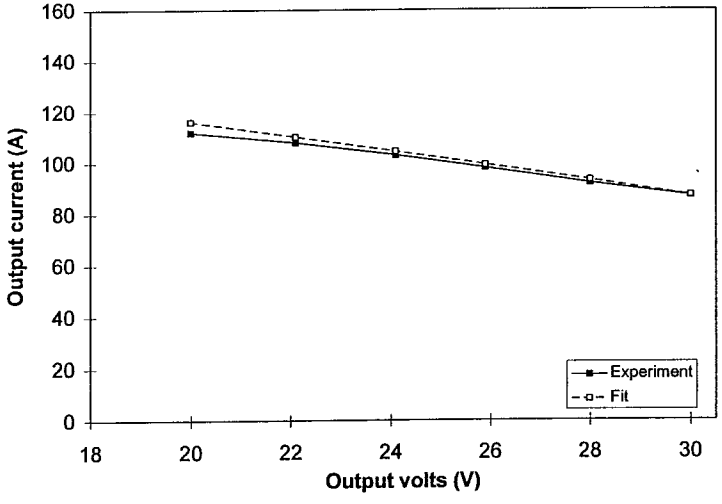

Figure 2.3b: Run 6, nominal 0.6 Torr, fitted as 0.45 Torr

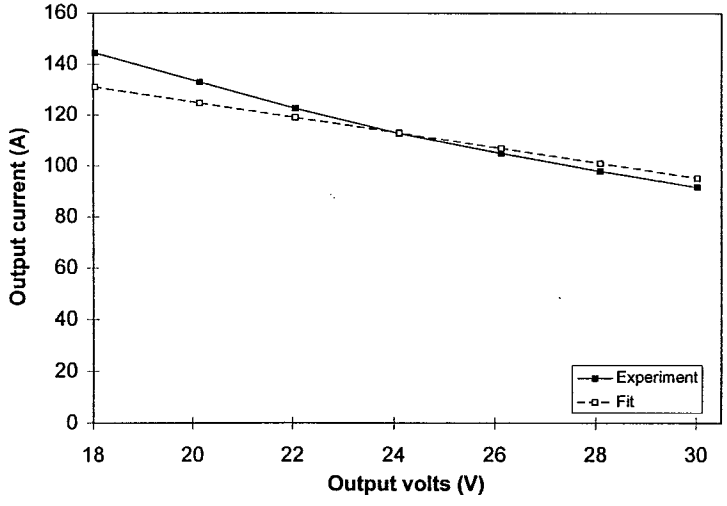

Figure 2.3d : Run 3, nominal 0.7 Torr, fitted as 0.46 Torr

Figure 2.3 : Thermal power = 95 kW, fitted by modifying Cs pressure

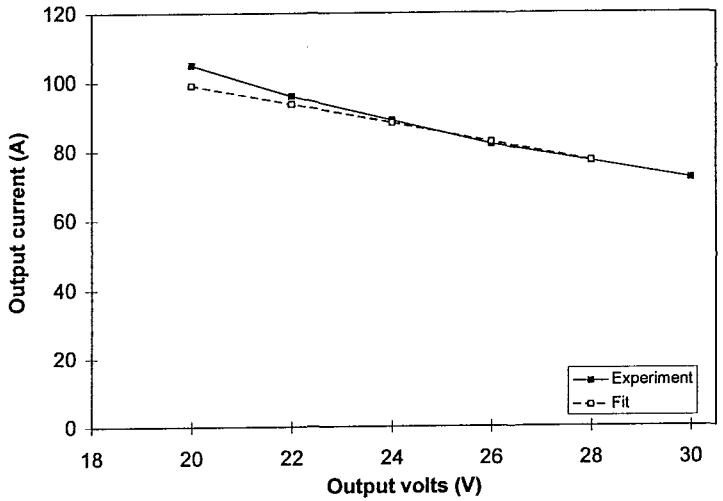

Figure 2.4a : Run 3, nominal 0.6 Torr, fitted as ϕ_E x 1.044

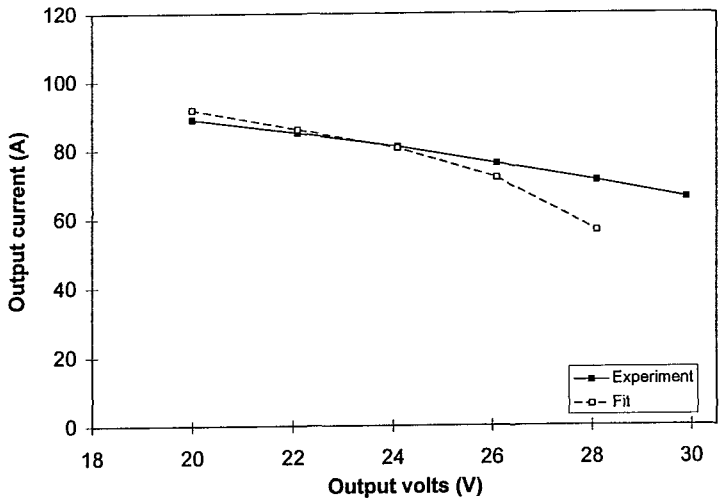

Figure 2.4b: Run 6, nominal 0.6 Torr, fitted as ϕ_E x 1.045

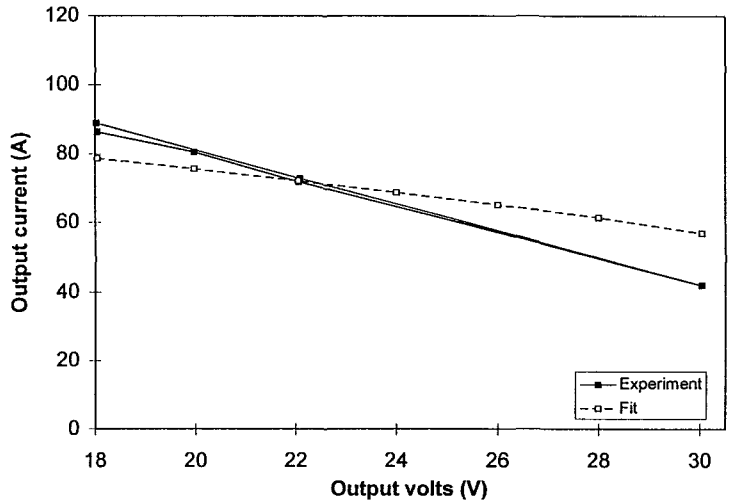

Figure 2.4c : Run 8, nominal 0.6 Torr, fitted as ϕ_E x 1.057

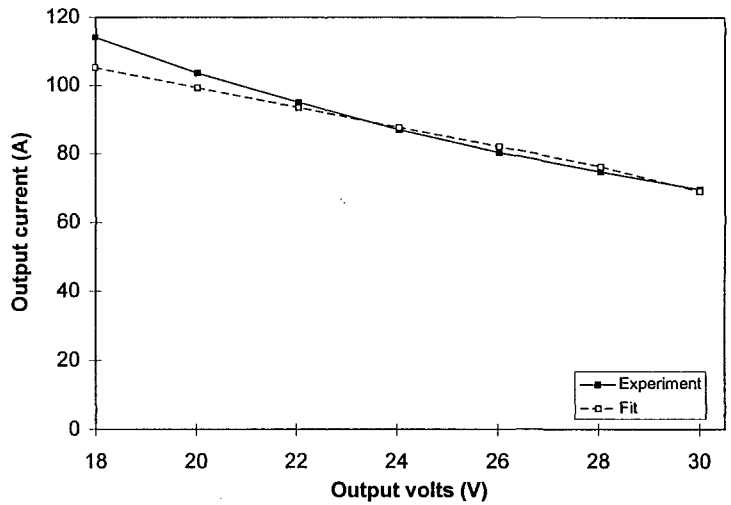

Figure 2.4d : Run 3, nominal 0.7 Torr, fitted as ϕ_E x 1.059

Figure 2.4: Thermal power = 85 kW, fitted by scaling emitter work function

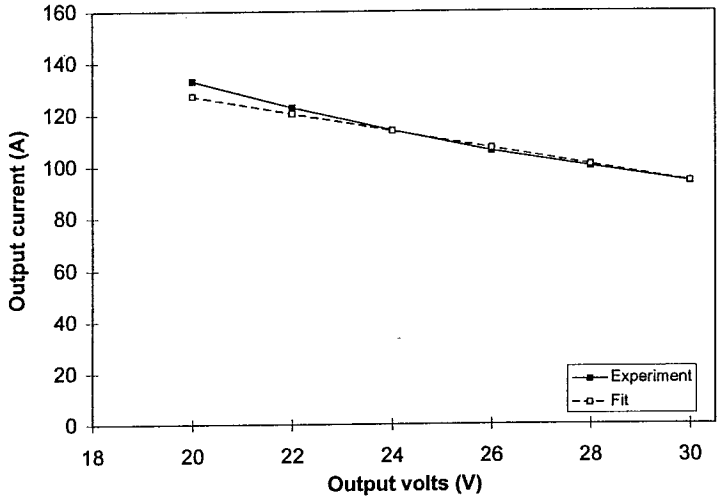

Figure 2.5a : Run 3, nominal 0.6 Torr, fitted as ϕ_E x 1.024

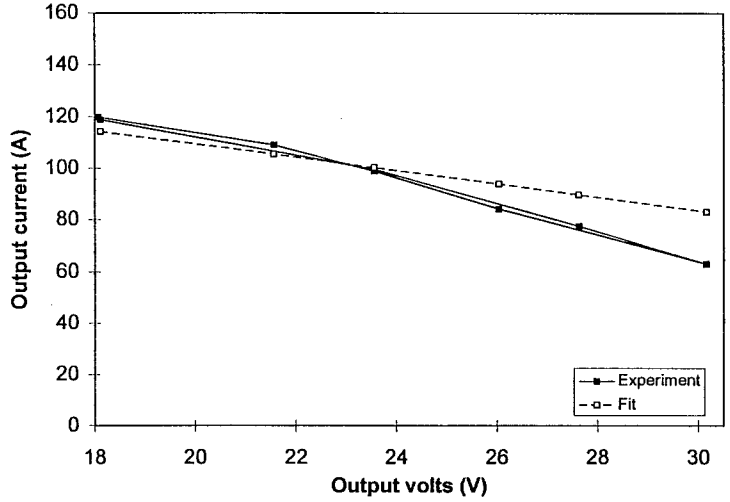

Figure 2.5c : Run 8, nominal 0.6 Torr, fitted as ϕ_E x 1.031

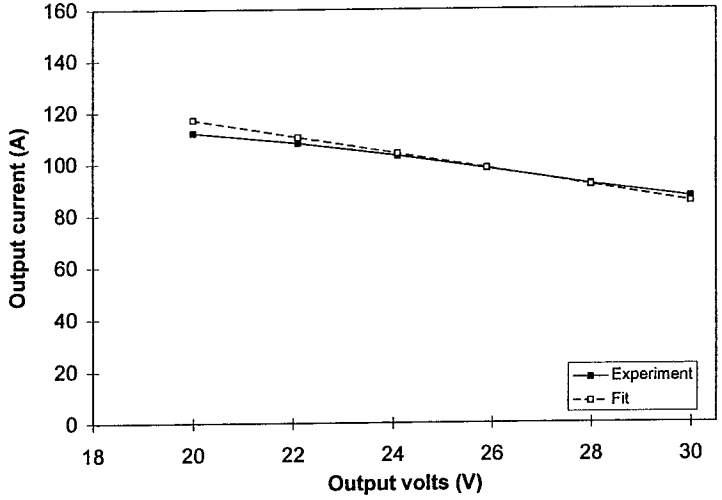

Figure 2.5b: Run 6, nominal 0.6 Torr, fitted as ϕ_E x 1.026

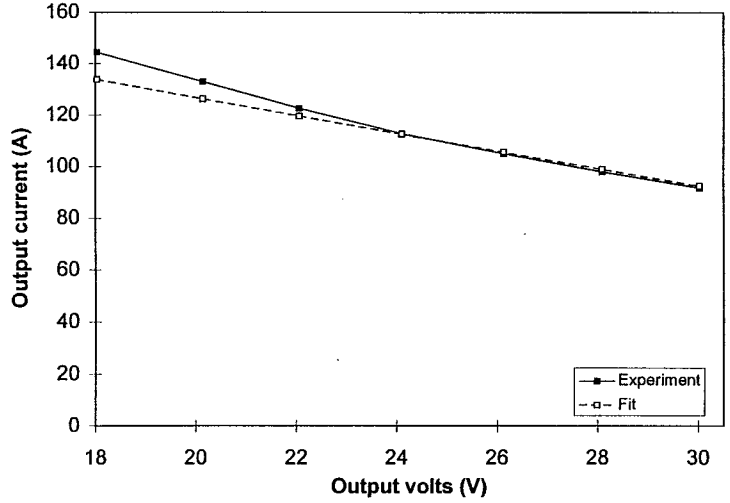

Figure 2.5d : Run 3, nominal 0.7 Torr, fitted as ϕ_E x 1.039

Figure 2.5: Thermal power = 95 kW, fitted by scaling emitter work function

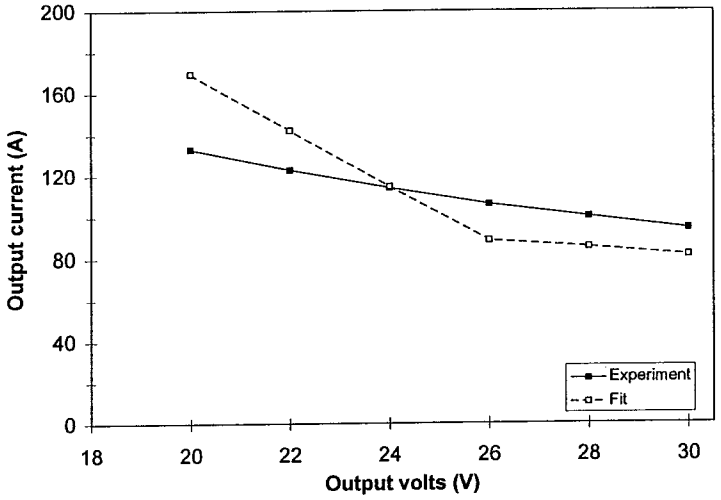

Figure 2.6a : 95 kW, nominal 0.6 Torr, fitted as ε_{eff} x 1.34

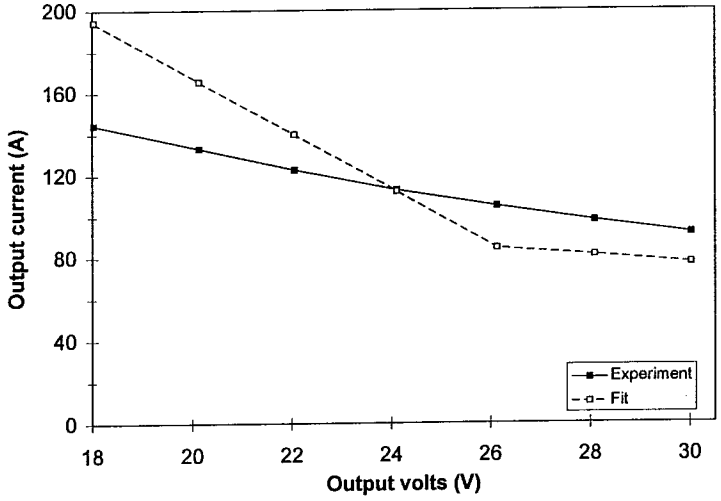

Figure 2.6b: 95 kW, nominal 0.7 Torr, fitted as ε_{eff} x 1.34

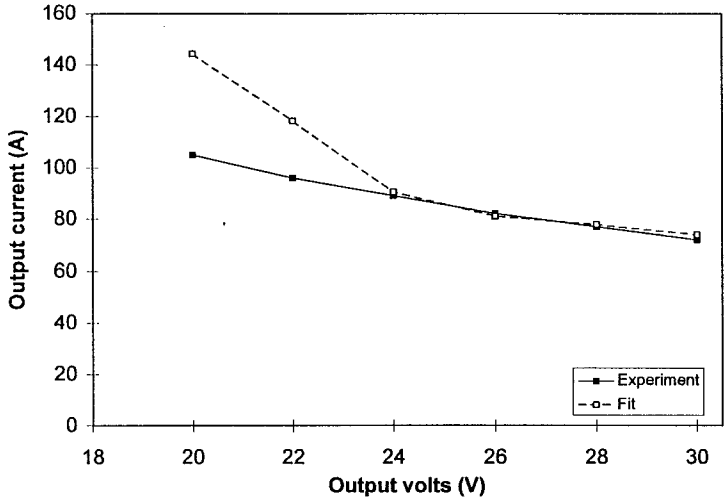

Figure 2.6c : 85 kW, nominal 0.6 Torr, fitted as ε_{eff} x 1.21

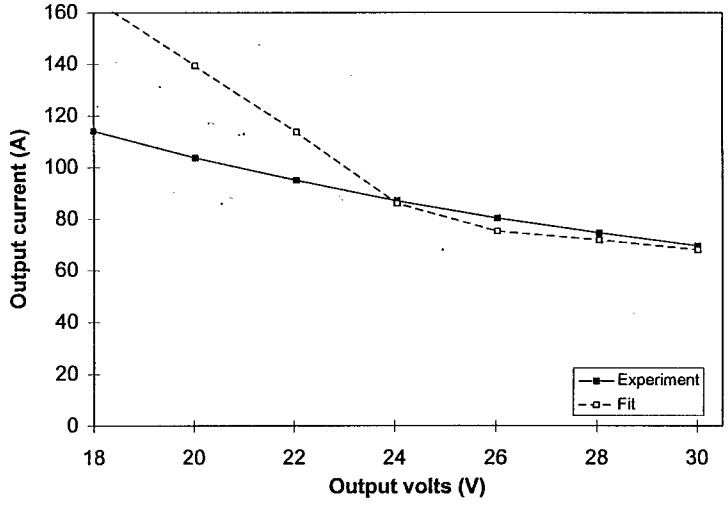

Figure 2.6d : 85 kW, nominal 0.7 Torr, fitted as ε_{eff} x 1.22

Figure 2.6: Run 3, fitted by scaling effective emissivity of inter-electrode gap

Section 3 - Code Documentation

3.1 Introduction

Three codes have been written in order to model the TOPAZ-II TFE output. They are called IV1D, EQ1D and NAK1D. They are all written in Fortran. The purpose of each of these is described in the first section of this report.

3.1.1 Symbols

Symbol	Name in code	Description
J_S'	JEMIDEAL	Emitter zero field electron emission (Richardson current density)
J_C	JCIDEAL	Collector zero field electron emission (Richardson current density)
ϕ_E	PHIEM	Emitter work function
ϕ_C	PHICOL	Collector work function
ϕ_S	PHIENEW	Emitter work function modified due to Schottky effect (sat. mode)
T_E	EMTEMP	Emitter temperature
T_C	COLTEMP	Collector temperature
P_{Cs}	PRES	Cesium pressure
T_R	TRES	Cesium reservoir temperature
T_{NaK}	TNAK	NaK coolant temperature
T_m	TMEAN	Mean of emitter and collector temperatures
T_{mw}	TMW	Weighted mean of emitter and collector temperatures
T_{eE}	TEMPEEM	Emitter electron temperature
T_{eC}	TEMPEC	Collector electron temperature
T_{em}	TEEMEAN	Mean of emitter and collector electron temperatures
d_g	DGAP	Interelectrode gap spacing
d/λ_{ea}	DULAMBDA1	Ratio of gap spacing to electron-neutral mean free path
d/λ_e	DULAMBDA	Ratio of gap spacing to electron mean free path
k_B	KB	Boltzmann's constant (= 8.617×10^{-5} eV K^{-1})
A	AA	Factor preceding Richardson equation (= 120.17266 A cm^{-2} K^{-2})
J_E	JEM	Electron emission from virtual emitter in obstructed mode
J_S	JSEM	Schottky modified emitter current density (in saturated mode)
ΔV	DELTAV	Emitter barrier height
V_{out}	VOUTWANT VOUT	Required output volts Calculated output volts
J_{out}	JOUT	Output current density
J_{unig}	JUNIG	Unignited mode output current density
J_{ix}/J_{out}	JIXRAT	Ratio of emitter ion current density to output current density (<0)
J_E/J_{out}	JERAT	
J_S/J_{out}	JSRAT	
J_C/J_{out}	JCRAT	

V_E	VEM	Emitter sheath height (V)
V_C	VCOL	Collector sheath height (V)
V_d	VD	Arc drop
V_{rad}	VRAD	Contribution to arc drop due to photon losses from plasma
R	R	Parameter involved in calculating J_E/J_{out}, J_S/J_{out}
ϕ_{nC}	PHINC	Equilibrium plasma potential
J_{nC}	JNC	LTE current density
q_{FUEL}	TPOWER	Thermal power to 1 TFE
Q_{FUEL}	QFUEL	Heat flux to emitter from fuel or TISA
Q_{in}	QIN	Heat flux from emitter into interelectrode gap
Q_{out}	QOUT	Heat flux into collector from interelectrode gap
Q_{NaK}	QNAK	Heat flux from collector to NaK
Q_{rad}	QRAD	Radiative heat flux from emitter to collector
Q_{Cs}	QV	Conductive heat flux from emitter to collector
Q_{eE}	QEE	Heat flux from emitter due to electron cooling
Q_{eC}	QEC	Heat flux to collector due to electron heating
ε_{eff}	EPSTFE	Effective emissivity of emitter
λ_{mw}	LAMBDA	Thermal conductivity of Cs vapour at T_{mw}
$\dot{m}$	MDOT	NaK mass flow rate
	EPSTNEW	Scaling factor for ε_{eff}
	EMCOR	Scaling factor for ϕ_E
	COLCOR	Scaling factor for ϕ_C

3.2 Code description

3.2.1 IV1D

This is a stand-alone I-V characteristic program. It involves no heat transfer calculations. It calculates J_{out} for the required V_{out}, given P_{Cs}, T_E and T_C. It calculates J_{out} for both ignited and unignited mode operation, and gives the final J_{out} as the higher of the two values. A schematic of the structure of the code is shown in figure 3.1. The function of each of the subroutines is described below. The reader should refer to the TECMDL and UNIG documentation (Rasor and McVey, Dahlberg *et. al.* 1994, Rasor Associates 1991) for further details of the equations used in these codes.

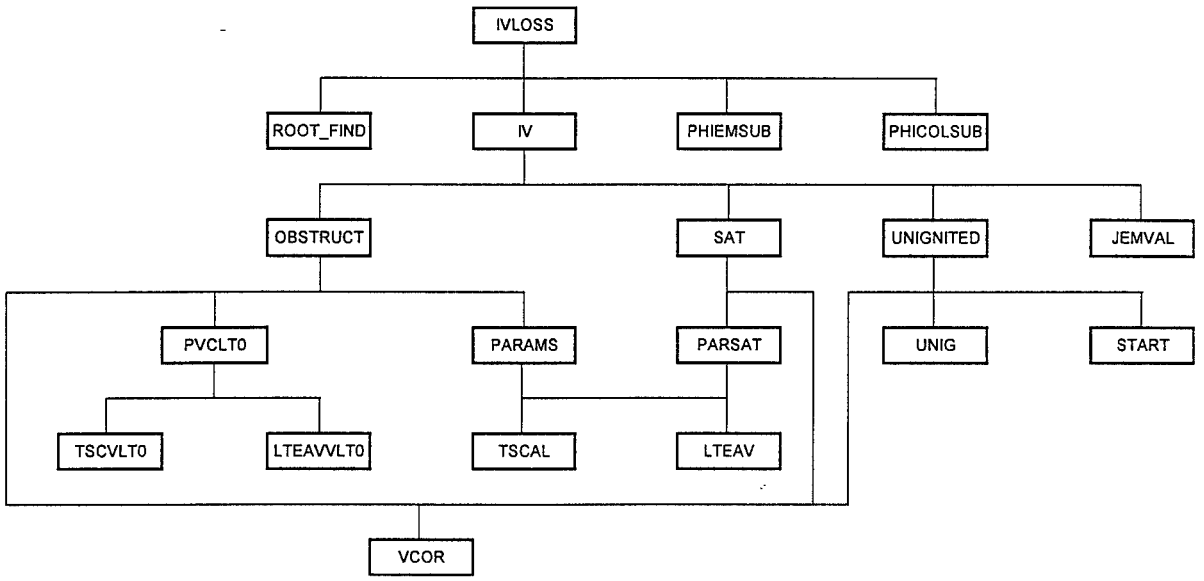

Figure 3.1 : Structure of IV1D program

Main program

P_{Cs}, T_E and T_C are entered. ROOT_FIND is called to calculate the equivalent Cs reservoir temperature (T_R) from P_{Cs}. The PHIEMSUB and PHICOLSUB subroutines are called to evaluate ϕ_E and ϕ_C. The mean of the emitter and collector temperatures, T_m is calculated and used to evaluate the ratio d/λ_{ea}. These values are used later in the I-V calculations. The required value of V_{out} is entered. The user has the option to include the effect of voltage drops in the electrodes. If they are included, the user is prompted for a NaK temperature. This is necessary as in the heat transfer codes the ends of the emitter and the collector are assumed to be at the same temperature as the NaK. This value is not used anywhere else in IV1D. The default NaK temperature used here is 25 K cooler than the collector temperature.

ROOT_FIND

Calculates the equivalent Cs reservoir temperature T_R to the Cs pressure P_{Cs}, using a Newton-Raphson iteration.

PHIEMSUB

This subroutine calculates ϕ_E from T_E and T_R. It also uses the Richardson equation (Hatsopoulos and Gyftopoulos 1973) to calculate the "ideal" emitter current density J'_S, assuming no additional voltage barriers to electron emission.

PHICOLSUB

Performs equivalent calculations for the collector.

JEMVAL

If the emitter barrier, ΔV, is greater than zero (i.e. in the obstructed region of the ignited mode), J_S' is scaled by a factor $\exp(-\Delta V/k_B T_E)$, to give the electron emission from the "virtual emitter", J_E.

IV

The main "control" code for calculating J_{out} (ignited or unignited mode) at the required V_{out}. It calls ignited mode calculations, and compares these J_{out} values with those from the unignited mode calculation. If the ignited mode does not have a solution at this required V_{out}, or if the unignited mode gives a higher J_{out}, the unignited mode is used. The following procedure is used. ΔV is set to zero and the OBSTRUCT subroutine is used to calculate V_{out} and J_{out} at the transition point (where the ignited mode switches from obstructed to saturated mode operation). It then sets $\Delta V = -1.0 \times 10^{-10}$ (i.e. saturated mode, very close to transition point) and finds V_{out} and J_{out} there. If the required V_{out} is between these two values, it uses a linear extrapolation between the two points to find the corresponding J_{out}. This linear extrapolation is used because points in this ΔV range can be difficult to find using an iterative method. The unignited mode current density (J_{unig}) is also calculated for the required V_{out} and if this value is larger it will be used as the value for J_{out}. Control then returns to the main program.

In most cases the required V_{out} will not fall in the range described above, in which case the following procedure is used. Since there are regions in which the ignited mode I-V characteristic does not exist, a check must be made of whether it does exist at the required V_{out}. The point in the obstructed mode at which the I-V characteristic ceases to exist is characterized by a region where, as ΔV is increased, V_{out} reaches a maximum and begin to decrease. This effect occurs because the model becomes non-physical in this region. The maximum voltage which can be obtained in the ignited mode calculation is found by increasing ΔV in progressively smaller increments and finding where the corresponding V_{out} begin to decrease. If the required V_{out} is larger than this value, the unignited mode is used and control is returned to the main program.

Having made these preliminary checks, a Newton-Raphson routine is used to iterate ΔV until the calculated value of V_{out} is equal to the required value. If the gradient of a plot of V_{out} against ΔV is found to be negative during this process, this corresponds to going above the maximum output volts for the ignited mode and the calculations is begun again at a smaller ΔV. If more than 20 loops are used in an iteration, the starting ΔV is made smaller and the sign changed, and a new iteration is started. Once a solution is found, it is compared with the unignited mode current density and the larger value taken as the output current density. The emitter electron cooling heat flux, Q_{eE}, is also taken from the ignited or unignited mode calculation as appropriate.

It should be noted that the quantity ΔV has been assigned both positive and negative values to correspond to the obstructed and saturated modes respectively. In the obstructed mode it equals the emitter barrier height. It does not have physical meaning in the saturated mode, but has been set up to have an artificial relationship with the quantity J_{ix}/J_{out}, which is varied to vary V_{out} in

the saturated mode calculation. Given the structure of the present code, compared with TECMDL, this is a more convenient approach and does not affect the calculated output current density.

OBSTRUCT

Uses a Newton-Raphson routine to solve the equation

$$\frac{J_E}{J_{out}} = 1 + \exp\left(-\frac{V_E}{kT_{eE}}\right)\left[\frac{3}{4}\frac{d}{\lambda_e} + R\right] ,$$

for a consistent value of J_E/J_{out}. It uses subroutines PARAMS if $V_C > 0$ or PVCLT0 if $V_C < 0$, to calculate the necessary parameters, some of which are a function of J_E/J_{out}. When convergence has occurred, it removes the electrode voltage losses from V_{out} and calculates Q_{eE}.

PARAMS

Calculates values needed in OBSTRUCT, specifically T_{eE}, T_{eC}, T_{em}, V_C, V_{rad}, V_d, V_E, V_{out}, R, d/λ_e and J_E/J_{out}. It also considers whether local thermodynamic equilibrium (LTE) considerations affect either T_{eC} alone or both T_{eC} and T_{eE}. Subroutine TSCAL is called first to check the value of T_{eC}. If the value of T_{eC} has to be modified, then subroutine LTEAV is called to change T_{eE} if this is also required.

PVCLT0

If PARAMS returns a value of $V_C < 0$, then this subroutine is used instead of PARAMS to calculate the parameters required in OBSTRUCT. If LTE considerations affect T_{eC} and T_{eE} subroutines TSCVLT0 and LTEAVVLT0 are used in the same way as PARAMS uses TSCAL and LTEAV.

SAT

If $\Delta V < 0$, then this subroutine is called after OBSTRUCT. It solves the equation

$$\frac{J_S}{J_{out}} = 1 + \exp\left(-\frac{V_E}{kT_{eE}}\right)\left[\frac{3}{4}\frac{d}{\lambda_e} + R - \frac{1}{2}\frac{J_{ix}}{J_{out}}\right] + \frac{J_{ix}}{J_{out}}$$

for a constant J_S/J_{out}. It uses PARSAT to calculate the necessary values for this iteration, some of which are a function of J_S/J_{out}. It then solves

$$J_S = J'_S \exp\left[\frac{612}{T_E}\left(\frac{J_{ix}}{J_{out}} J_{out}\sqrt{V_E}\right)^{\frac{1}{4}}\right]$$

for a constant J_{out}. The value of J_{ix}/J_{out} is given by

$$\frac{J_{ix}}{J_{out}} = \frac{\Delta V}{5}$$

When convergence has occurred, it subtracts the electrode voltage losses from V_{out} and calculates Q_{eE}.

PARSAT

Calculates the values needed for the first iteration in SAT, specifically T_{eE}, T_{eC}, T_{em}, V_C, V_{rad}, V_d, V_E, V_{out}, R, d/λ_e and J_S/J_{out}. In testing this I-V characteristic over a wide range of conditions, no case has arisen in the saturated mode where $V_C < 0$, so this capability has not been included in this model. If this situation does arise, a comment will appear on the screen and the program will pause. This case may only arise under operating conditions far removed from those relevant to TOPAZ-II. As in PARAMS, tests for LTE restrictions are used. TSCAL and LTEAV are used in an analogous manner to their use in PARAMS.

TSCAL

In order for LTE to be satisfied at the collector, T_{eC} must be greater than or equal to the value defined by LTE restrictions. If this is not the case for the value calculated in PARAMS, it is replaced by the LTE limited value, calculated using equations 5, 9, 12 and 13 of McVey and Rasor. (Following references to equation numbers are all from McVey and Rasor).

LTEAV

If T_{eC} was constrained by LTE, the value of T_{em} may also be restricted. This in turn changes both T_{eE} and T_{eC}. This calculation uses equations 8 and 9 in calculating the new value for T_{em}, then calculates the new T_{eC} using the same procedure as in TSCAL. It should be noted that the substitution $T_{eE} = 2T_{em}-T_{eC}$ has been used in equation 5 for the LTE restricted value of T_{eC}.

TSCVLT0

Performs the same function as TSCAL, but is used by PVCLT0 for cases when $V_C < 0$. Calculates the LTE restricted value for T_{eC} using the equation applicable for $V_C < 0$.

LTEAVVLT0

Performs the same function as LTEAV, but is used by PVCLT0 for cases when $V_C < 0$. Calculates T_{eC} using the equation applicable for $V_C < 0$. The substitution $T_{eE} = 2T_{em}-T_{eC}$ has again been used in equation 20 for the LTE restricted value of T_{eC}.

VCOR

Calculates the internal voltage drop in the TFE as a result of resistive losses in the emitter and collector. If the user has chosen not to include voltage drops, it returns a value of zero.

UNIGNITED

Performs iterations to find J_{unig} at the required V_{out}, using UNIG to calculate V_{out} corresponding to a given J_{unig}. It first finds the value of V_{out} at which $J_{unig} = 0$. If the required V_{out} is greater than this value, it returns a current density of zero. If this is not the case it then uses the START subroutine to find a value of J_{unig} producing a voltage less than V_{out}. A linear extrapolation between these points is used to find a suitable starting value of current density for the iterative procedure. At current densities above a certain value, which depends on the TFE operating parameters, UNIG cannot find a corresponding V_{out}. When this is the case, it returns a value of -99. If the required (J_{unig}, V_{out}) point is very close to this limit, the Newton-Raphson procedure may "hit" points in this non-physical region. This is why the initial extrapolation to find a starting point close to the required solution is used. If an error does occur in the Newton-Raphson iteration a bisection procedure is used to find the solution. UNIG also returns a value for Q_{eE} which is used in the heat transfer calculations.

If START cannot find a value of J_{unig} large enough to produce a voltage less than V_{out}, a linear extrapolation is used from two current values just less than the value at which UNIG ceases to find a corresponding voltage. An extrapolated value for Q_{eE} is also found.

START

Looks for a point on the I-V characteristic with output volts less than the required V_{out}. It increases J_{unig} from zero using progressively smaller increments to find a suitable point. If it finds a potentially suitable point it moves to a slightly value of J_{unig} and calculates J_{unig}, V_{out} pairs at 10 points up to the value initially chosen as a suitable starting point. It then checks that there are no discontinuities in the I-V characteristic in this region, by looking for anomalously large changes in V_{out} between successive points. It has been found in tests that in the region close to where UNIG cannot return a value for V_{out}, some discontinuities can occur. If a discontinuity is detected, the new starting point is set to a J_{unig} value just below this point. If the closest starting point which can be found still produces a value for V_{out} greater than the required value, a logical variable is set so that the extrapolation procedure is used in UNIGNITED.

UNIG

This subroutine is unchanged from McVey's version (Rasor Associates 1991), except that all floating point variables have been declared as double precision, to be consistent with all the other subroutines. It calculates V_{unig} corresponding to a given J_{unig}, for the unignited mode of TFE operation.

3.2.2 NAK1D

NAK1D calculates T_E, T_C and J_{out} for a TOPAZ-II TFE under physically reasonable operating conditions. Once the equilibrium condition has been found, it is possible to change T_{NaK} and find the new equilibrium T_E, T_C and J_{out}. The structure of the code is shown in figure 3.2. The I-V characteristic calculation is the same as that used in IV1D and will not be described further. In the schematic, the subroutine "IV" is taken to mean both that subroutine and all other ignited and unignited mode subroutines.

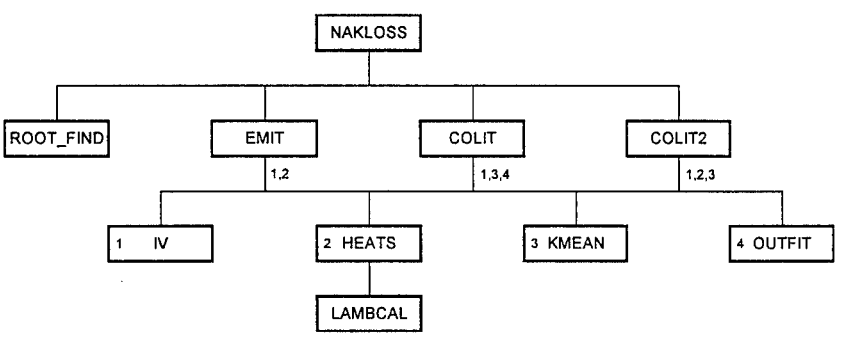

Figure 3.2 : Structure of NAK1D program

Main Program

NAK1D has been set up to read its input values from a file, VALUES.DAT. The file contains values for P_{Cs}, the TISA power for one TFE, q_{FUEL}, the NaK mass flow rate, $\dot{m}$, starting values for T_E and T_C, the required V_{out}, the option of including or neglecting electrode voltage drops, and scaling factors for ϕ_E, ϕ_C and the effective emissivity of the interelectrode gap. A scaling factor of 1.00 leaves that quantity unchanged from its default value. The heat flux from the TISA to the emitter, Q_{FUEL}, is calculated from the TISA power. All values in this file must have a decimal point, if integers are present they will be misinterpreted by the program. The value of $\dot{m}$ is for a single TFE, and is therefore 1/37 of the value for the NaK flow rate through the EM pump. Subroutines EMIT and COLIT are called alternately to find the equilibrium values of T_E and T_C respectively. After each pass through this pair of subroutines the user has the option of doing another pass or stopping at that point. With each pass through these subroutines the values of T_E, T_C and J_{out} get closer to a consistent value. After this part of the program is completed the user has the option to change T_{NaK} from the value which has already been calculated. If this option is chosen, the subroutines COLIT2 and EMIT are used alternately until a new equilibrium set of values for T_E, T_C and J_{out} are found. Under conditions where the TFE is close to the

transition between the ignited and unignited modes of operation, the value of T_E or T_C may not converge. If this occurs, the user should change the starting values of T_E and/or T_C. If the calculation still does not converge, the only solution is to make a small change to one of the operating parameters, for example the thermal power or the output volts.

EMIT

Calculates the equilibrium value of T_E. It uses IV to return the value for Q_{eE} and HEATS to return the heat flux from the emitter into the interelectrode gap, Q_{in}. A Newton-Raphson iteration is used to find the value of T_E where Q_{in} is equal to Q_{FUEL}. The collector is assumed to be at equilibrium in this part of the calculation.

COLIT

Calculates the equilibrium value of T_C. It uses IV to return J_{out} and calculates the heat flux to the collector, Q_{out} as the difference between Q_{FUEL} and the output power density. The emitter is assumed to be at equilibrium in this part of the calculation. T_{NaK} is calculated from Q_{out} using OUTFIT. The heat flux to the NaK, Q_{NaK} is calculated using KMEAN. A Newton-Raphson iteration is used to find the T_C where Q_{out} is equal to Q_{NaK}.

COLIT2

Calculates the equilibrium value of T_C after T_{NaK} has been changed by the user. T_{NaK} is now fixed. It uses IV to return J_{out} and Q_{eE} and HEATS to calculate Q_{out}. Q_{NaK} is calculated using KMEAN. A Newton-Raphson iteration is used to find the T_C where Q_{out} is equal to Q_{NaK}. The emitter is again assumed to be at equilibrium.

HEATS

Calculates the values of the heat fluxes across the interelectrode gap, Q_{rad}, Q_{eE}, Q_{eC} and Q_{Cs}. It also calculates Q_{NaK} using KMEAN. Convective heat transfer to the NaK is also included in this term. The effective emissivity, ε_{eff} is calculated using the current value of T_E. The value of Q_{eE} returned by the IV subroutine is used to calculate Q_{eC}. The weighted mean temperature T_{mw} is calculated and used in LAMBCAL to find the thermal conductivity of the Cs vapour, λ_{mw}. Finally values of the total heat flux from the emitter Q_{in} and to the collector Q_{out} are found.

LAMBCAL

Calculates λ_{mw} for a given T_{mw} and P_{Cs}.

OUTFIT

Calculates T_{NaK} from Q_{out}, using the calibration produced using the program EQ1D. A slightly different calibration is used depending on whether electrode voltage drops are included.

KMEAN

Calculates the value of Q_{NaK}. The convective heat transfer to the flowing NaK is also included in this term. The thermal conductivities of the plasma-sprayed alumina, He gap and stainless steel NaK channel wall are calculated from the relevant calibrations of thermal conductivity versus temperature. Since the He gap provides the greatest thermal resistance, the plasma-sprayed alumina is taken to be at T_C, the He gap is taken to be at the mean of T_C and T_{NaK}, and the stainless steel wall is taken to be at T_{NaK}.

3.2.3 EQ1D

The structure of this program is very similar to NAK1D. It is used to produce the calibration between Q_{out} and T_{NaK} used in NAK1D. It uses experimental data of the relationship between q_{FUEL} and T_{NaK} to fix T_{NaK} for a calculation at a given q_{FUEL}. The value of Q_{out} produced by this program is paired with the T_{NaK} value, as described in section 1 of this report. The code does not include the option to change T_{NaK}, available in NAK1D. The only parts of the program which are different from NAK1D are the main program and subroutine COLIT2. Subroutines POWFIT and POWFIT2 are only present in EQ1D. Subroutines COLIT and OUTFIT from NAK1D are not present. Only the parts which are different are described below. The I-V characteristic calculation is the same as in IV1D. A schematic of the structure of EQ1D is shown in figure 3.3.

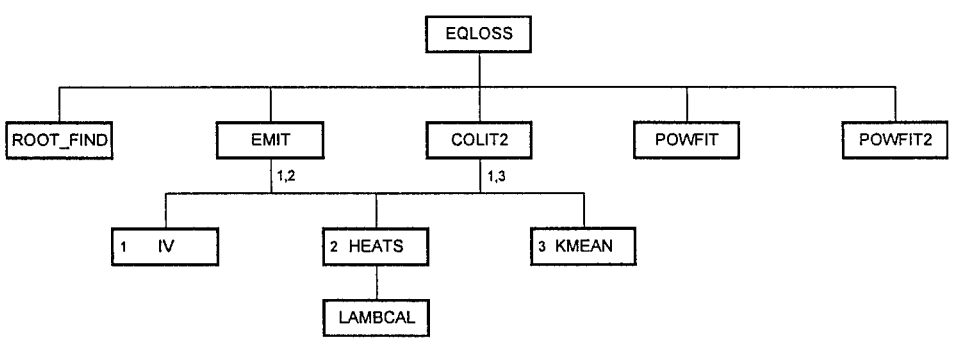

Figure 3.3 : Structure of EQ1D program

Main Program

EQ1D reads its input values from the same file, VALUES.DAT, as NAK1D. The only difference is that once the value for q_{FUEL} has been read in, subroutines POWFIT and POWFIT2 are called to return values for T_{NaK} at the reactor outlet and inlet respectively. The mean of these two values is calculated and used as the fixed value for T_{NaK} through the rest of the program.

COLIT2

Calculates the equilibrium value of T_C. It uses IV to return J_{out} and calculates Q_{out} as the difference between Q_{FUEL} and the output power density. Q_{NaK} is calculated using KMEAN. A Newton-Raphson iteration is used to find the T_C where Q_{out} is equal to Q_{NaK}. The emitter is assumed to be at equilibrium.

POWFIT

Calculates T_{NaK} at the reactor outlet from q_{FUEL}.

POWFIT2

Calculates T_{NaK} at the reactor inlet from q_{FUEL}.